Dynamic Performance Assessment of Primary Frequency Modulation for a Power Control System Based on MATLAB

Shizhe Li *[ID] **and Yinsong Wang**

School of Control and Computer Engineering, North China Electric Power University, Baoding 071003, China; missliujinmei@163.com
* Correspondence: 52651488@ncepu.edu.cn; Tel.: +86-312-752-3460

Abstract: The primary frequency modulation (PFM) performance of a power control system (PCS) is an important factor affecting the security and stability of a power grid. The traditional control method is proportional integral (PI) control. In order to improve its dynamic control performance, a control method based on the combination of internal model control (IMC) and PI is proposed. Using the method of theoretical assessment and system identification, a simple simulated model of the typical PCS is established. According to the principle of system identification and the least square estimation (LSE) algorithm, the mathematical models of a generator and a built-in model are established. According to the four dynamic performance indexes, the main and auxiliary assessment index of the PCS are defined, and the benchmark and the result of the performance assessment are given. According to three different structures, the PFM dynamic performance of the PCS is analyzed separately. According to the dynamic performance assessment index of PFM, the structure of the control system and the influence of different parameters on the performance of the PCS are analyzed under ideal conditions. The appropriate control structure and controller parameters are determined. Secondly, under the non-ideal condition, the influence of the actual valve flow coefficient on the performance of the control system is studied under two different valve control modes. The simulation results show that the internal model combined with PI has better dynamic control performance and stronger robustness than the traditional PI control, and it also has better application prospects for thermal power plants.

Keywords: dynamic performance assessment index; power control system; primary frequency modulation; least square estimation; internal model control; valve local flow coefficient

1. Introduction

Power grid frequency is an important index of power quality that reflects the balance relation between active power and load. Controlling the frequency of a power grid makes it maintain a rating, which is an important task for power grid operation. Frequency control of the power grid consists of three stages according to execution order, namely primary frequency modulation (FM) (please refer to Abbreviation list for all abbreviations appearing in this article), secondary FM, and triple FM. The frequency control function at all levels is cross-sectional and completes the power frequency the control task together. Among them, the primary frequency modulation (PFM) response time is fastest, so it is very important to restrain frequency fluctuation frequently, changing within small range and frequency stability when electric network accidents occur [1,2]. When power grid frequency deviates from the rated frequency, the thermal power units utilizing boiler heat storage respond quickly to the frequency change of a power grid, while the generator increases or decreases the output force

correspondingly, which is the PFM of the thermal power units. The rated speed of turbine generator is 3000 r/min, so the frequency of power grids is 50 Hz in China. At present, frequency variation of a power grid is permitted to be 0.1 Hz in developed countries, while it is 0.2 Hz in China. The influence of a photovoltaic power generation system and conventional hydropower generation on the frequency of a power grid is discussed in [3]. In the process of grid connection, the contribution of wind farms to frequency control is discussed in [4]. Because the thermal power units occupy a very important position in China's energy structure proportion, this paper mainly studies the effect of thermal units on the PFM performance of a power grid. Therefore, the performance of PFM is an important guarantee to prevent large fluctuations in frequency and to maintain grid stability. A sudden accident occurs if the network unit FM response ability is poor, and frequency fluctuation of a power grid is high when system collapse occurs. Under the trend of interconnection of regional power grids, the performance of PFM becomes more obvious. Many studies indicate that PFM plays an important role in maintaining stability under abrupt disturbances [5,6].

A mathematical model should be established for studying the PFM of a power control system (PCS). Previous studies mainly use mechanism assessment methods and system identification methods to describe models of dynamic characteristics of PCSs as much as possible [7,8]. Results show that a model is not only complex but also difficult to solve. Therefore, establishing a simplified PCS model with certain accuracy has become the primary task in studying the dynamic performance of PFM of generating units. Relevant studies have been carried out, and simplified models with certain accuracy have been established for steam turbines and generators [9,10]. Before a frequency disturbance test, the unit is in stable equilibrium state. When frequency disturbance is added, the turbine regulation speed changes quickly and the main steam pressure changes rapidly, according to the steam flow entering the steam turbine. Compared with the steam turbine, the boiler dynamic response is slower. During this process, the main steam pressure cannot maintain stability. Theoretically, the main steam pressure can change by establishing a boiler model, but this requires extra tests to identify boiler model parameters, and the boiler structure is very complicated. Perfect characterization of main steam pressure variation characteristics with a model is difficult, and the modeling cost is relatively high. When the turbine valve flow characteristic deviates from the ideal value, it may cause continuous power oscillation in the turbine generator, thereby triggering forced power oscillation of the power grid. Forced power oscillation caused by valve flow characteristics indicates that steam turbine valve flow characteristics not only affect the safety of a unit but also affect the stability of the power grid. The valve flow characteristics of the actual unit are tested, correcting the valve flow function. Optimizing the valve flow characteristics of the unit can reduce forced power oscillation accidents caused by imperfect valve flow characteristics [11,12]. However, during actual operation, valve flow characteristics may change over time, so valve flow function cannot guarantee reliable matching with the actual unit valve flow characteristics. Therefore, we modified and adjusted existing control strategies to restrain forced power oscillation caused by valve flow characteristics.

A thermal power plant is mainly composed of a thermal control system and a power generation system. A thermal control system mainly refers to boiler equipment and control loops, and a power generation system mainly refers to steam turbine and generator equipment control loops. In this paper, the PCS on the generator side is studied. In recent years, China's power system has developed rapidly, the scale is expanding, and the structure is becoming increasingly complex. As PFM is an important function of thermal power units related to the power grid, its performance has a direct impact on the security and stability of the power system [13–16]. Although an increasing amount of attention has been paid to the work of thermal power units related to the power grid, the design of the control system has not adapted to new situations with the demand of PFM and PCS, and the performance of some units is still not up to the expected value. In [17–19], the authors point out that the response time, regulation speed, and regulation range of a PCS are closely related to the control mode of the unit. Therefore, the design of a PCS is an important factor, affecting the performance of units and the power grid. In [20,21], it is shown that the configuration of the valve flow function has a significant

influence on the regulating effect of the thermal power unit control system. In [22,23], it is pointed out that the variation in operating characteristics not only affects the performance of the existing control system, but also endangers the safety and stability of the unit in the process of operation. In [24–27], it is pointed out that the control strategy of each control loop in the power plant generally adopts the proportional integral (PI) control structure. The main reason is that the PI control strategy has strong robustness, and it is easy to adjust parameters. Therefore, new control algorithms, such as internal model control (IMC) [28–30] and the intelligent control algorithm [31–33], even if the development is very rapid, are of very little practical application for a control system of thermal power plants with such high security requirements. A small number of applications are limited to local control loops. IMC is a highly practical method proposed in the 1980s. An extension of the Smith predictor, it has a simple structure, a simple design, fewer online adjustment parameters, a clear adjustment policy, and easy adjustability. The improvement in robustness and disturbance as well as the effect especially on the control of a large time-delay system are especially remarkable. Therefore, it is not only used in slow response process control, but also has a better effect in the fast response of motor control compared with the PI control algorithm since its advent. In order to optimize the performance of the PCS, a PCS based on IMC is proposed in this paper. For simplicity and practicality, this paper does not establish a boiler side main steam pressure model. With adopting a mathematical model of the turbine generator, the simulated model of the PCS is built in a MATLAB environment. First, under ideal conditions, the valve local flow coefficient is supposed as 1. The dynamic performance of PCSs under different control strategies and controller parameters is studied. Second, according to two kinds of steam turbine valve control modes, the actual valve local flow coefficient is calculated, and the dynamic characteristics and robustness of a PCS under different control strategies are analyzed. In a simulated environment, the performance of the IMC system and the PI control system are compared. The simulation results show that the control strategy based on the combination of the internal model and PI control can better ensure the control performance of the unit under the operating characteristics and operation mode changes. Thus, the performance of the PFM of the unit is improved, and the security and stability of the power system are improved.

The organizational structure of this paper is as follows. In Section 2, the methods are introduced. In Section 3, the working principle of the PCS and the mathematical model of each component are introduced in detail. In Section 4, four indexes are defined as the benchmark of the performance assessment. On this basis, the factors that affect the PCS are simulated in detail, and the performance of the system is compared and analyzed. In Section 5, the valve local flow coefficient is defined, and the relationship between different valve control modes and the valve local flow coefficient is analyzed. At the same time, under the simulation environment, when the valve local flow coefficient is different, the performance of the PCS in PI and IMC mode is compared and analyzed, the root locus is plotted, and the robustness of the system is analyzed. Section 6 summarizes the paper.

2. Methods

2.1. Control System Based on Proportion Integration Differentiation

Figure 1 is a schematic diagram of the traditional proportion integration differentiation (PID) control system.
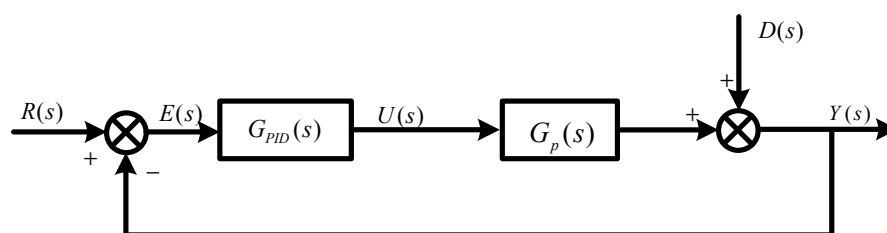

Figure 1. Schematic diagram of the proportion integration differentiation (PID) control system.

In Figure 1, $G_P(s)$ and $G_{PID}(s)$ represent the controlled object and controller, respectively, and $R(s)$, $E(s)$, $U(s)$, $Y(s)$, and $D(s)$ represent the reference, the error, the control action, the output, and the external disturbance, respectively.

The mathematic relationship between input and output of the PID controller is as follows:

$$u(t) = K_P e(t) + K_I \int_0^t e(t)dt + K_D \frac{de(t)}{dt}. \tag{1}$$

The corresponding transfer function is as follows:

$$G_{PID}(s) = \frac{U(s)}{E(s)} = K_P + \frac{K_I}{s} + K_D s = K_P(1 + \frac{1}{T_I s} + T_D s). \tag{2}$$

2.2. The Structure and Design of IMC

The structure of the IMC system is shown in Figure 2. $G_P(s)$ is the process, $\hat{G}_P(s)$ is the controlled object model, and $G_{IMC}(s)$ is an IM (internal model) controller. $R(s)$, $U(s)$, $Y(s)$, $Y_m(s)$, and $D(s)$ represent the reference, the control action, the object output, the model output, and the external disturbance, respectively.
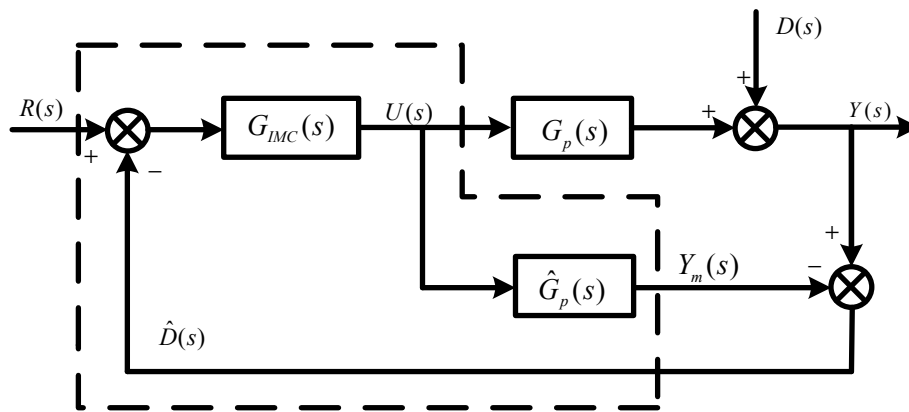

Figure 2. Schematic diagram of the internal model control (IMC) system.

In Figure 2, we can obtain the following relation between the equivalent feedback controller $G_c(s)$ and the IM controller $G_{IMC}(s)$ in the dashed line:

$$G_c(s) = \frac{G_{IMC}(s)}{1 - G_{IMC}(s)M(s)}. \tag{3}$$

The internal model controller is transformed into a PID-type solution; that is, Equation (2) is equivalent to Equation (1). Therefore, the PID controller is designed from the point of view of IMC. In general, the design process of an internal model controller is as follows:

(A) The model $G_p(s)$ of the controlled object is decomposed into an all-pass part $G_{p_+}(s)$ and a minimum phase part $G_{p_-}(s)$:

$$G_p(s) = G_{p_+}(s) \times G_{p_-}(s). \tag{4}$$

In Equation (2), $G_{p_+}(s)$ contains the pure lag element in $G_{p_-}(s)$ and the zero point of the right half s plane and

$$\left| G_{p_+}(s)(j\omega) \right| = 1 \qquad \forall \omega. \tag{5}$$

In general, $G_{p_+}(s)$ has the following form:

$$G_{p_+}(s) = e^{-\tau s} \prod_i \frac{-s + \xi}{s + \xi^H} \mathrm{Re}(\xi), \tau > 0. \tag{6}$$

In Equation (6), the superscript H denotes a complex conjugation.

(B) In order to suppress the influence of the model error on the system and increase the robustness of the system, a low-pass filter $G_{DT}(s)$ is added to the controller, which is generally taken as the simplest form as follows:

$$G_{DT}(s) = \frac{1}{(\lambda s + 1)^r}. \tag{7}$$

In Equation (7), the order r depends on the order of $G_{p_-}(s)$ so that the control can be realized, and λ is a time constant.

The IM controller obtained by this two-step design is as follows:

$$G_{IMC}(s) = G_{p_-}^{-1}(s) G_{DT}(s). \tag{8}$$

Substitute Equation (7) into Equation (8) and the result to Equation (3), and take Equation (4) into account. The following equation is then obtained:

$$G_c(s) = \frac{G_{p_-}^{-1}(s)}{(\lambda s + 1)^r - G_{p_+}(s)}. \tag{9}$$

When the process model is known, the parameters of the PID controller based on IMC can be obtained by Equations (2) and (9) according to the principle of identical equality.

If the controlled plant is an n-order model, the form of the state equation is given as follows:

$$\begin{aligned} X &= AX + Bu \\ Y &= CX \end{aligned}. \tag{10}$$

Under the optimal condition of the quadratic performance index,

$$J(u) = \frac{1}{2} \int_0^{t_f} \left(X^T G_{IMC} X + u^T R u \right) dt \rightarrow \min. \tag{11}$$

The following Hamiltonian function is obtained:

$$H = \frac{1}{2} X^T G_{IMC} X + \frac{1}{2} u^T R u + P^T (AX + Bu). \tag{12}$$

where P is the adjoint of the state vector:

$$P(t) = |X(t)| X^{-1}(t). \tag{13}$$

According to $\partial H / \partial u = 0$, the optimal control solution is

$$u^*(t) = -R^{-1} B^T P(t) = -K(t) X(t). \tag{14}$$

$$K(t) = R^{-1} B^T M(t). \tag{15}$$

The $M(t)$ is the solution of the following Riccati equation:

$$M(t) = -M(t)A - A^T M(t) + M(t) BR^{-1} B^T M(t) - G_{IMC}. \tag{16}$$

The Riccati equation has the following properties:

$$\lim_{t \to \infty} M = 0. \tag{17}$$

For the above reasons, the matrix differential equation of Equation (16) can be replaced by the following matrix differential equation:

$$MA = A^T M - MBR^{-1}R^T M + G_{IMC} + M(t)BR^{-1}B^T M(t) - G_{IMC}. \tag{18}$$

It can be seen from the viewpoint of modern control theory that PID is the optimal control model of process control for an n-order system, which shows that the PID controller designed based on the internal model principle also conforms to the principle of quadratic optimal control selection.

2.3. Least Squares Method (LSM)

In the process of establishing the whole mathematical model of the PCS, a system identification method is needed, and the most basic method is the LSM. Compared to other approaches, least square estimation (LSE) is easy to understand and often effective.

Since the sampling is discrete, the discrete model is usually used in time domain identification. Let the difference equation be

$$\sum_{i=0}^{n} a_i z(k-i) = \sum_{i=0}^{n} b_i u(k-i) \ , \quad a_0 = 1 \tag{19}$$

where u = input, z = output, and n = model order, respectively. In practical engineering, both input and output have measurement errors, and a noise is added to the previous equation:

$$y(k) = -\sum_{i=0}^{n} a_i z(k-i) + \sum_{i=0}^{n} b_i u(k-i) + e(k). \tag{20}$$

If there are $N + m$ points of measurement, there are N equations as follows:

$$
\begin{aligned}
y(n+1) \quad &= -a_1 y(n) - a_2 y(n-1) - \cdots - a_n y(1) \\
&\quad + b_0 u(n+1) + \cdots + b_n u(1) + e(n+1) \\
y(n+2) \quad &= -a_1 y(n+1) - a_2 y(n) - \cdots - a_n y(2) \\
&\quad + b_0 u(n+2) + \cdots + b_n u(2) + e(n+2) \\
\cdots \quad &\quad \cdots \\
y(n+N) \quad &= -a_1 y(n+N-1) - a_2 y(n+N-2) - \cdots - a_n y(N) \\
&\quad + b_0 u(n+N) + \cdots + b_n u(2) + e(n+2)
\end{aligned}
\tag{21}
$$

The above equations are written in vector form. The definition is as follows:

$$
\left\{
\begin{aligned}
&Y = [y(n+1), y(n+2), \cdots, y(n+N)]^T \\
&\varepsilon = [e(n+1), e(n+2), \cdots, e(n+N)]^T \\
&\theta = [a_1, a_2, \cdots, a_n, b_0, b_1, \cdots, b_n]^T \\
&\Phi = \begin{bmatrix}
-y(n) & \cdots & -y(1) & u(n+1) & \cdots & u(1) \\
-y(n+1) & \cdots & -y(2) & u(n+2) & \cdots & u(2) \\
\vdots & \vdots & \vdots & \vdots & \vdots & \vdots \\
-y(N+n-1) & \cdots & -y(N) & u(n+N) & \cdots & u(N)
\end{bmatrix}
\end{aligned}
\right. .
\tag{22}
$$

The equation can be written as

$$Y = \Phi\theta + \varepsilon. \tag{23}$$

That is,

$$\varepsilon = Y - \Phi\theta. \tag{24}$$

Define another objective function to measure the quality of the model:

$$J = \varepsilon^T \varepsilon. \tag{25}$$

Select a set of vectors $\hat{\theta}$ to minimize the objective function, i.e., to optimize. Place Equation (24) into Equation (25), and the objective function J is expressed as

$$J = (Y - \Phi\theta)^T(Y - \Phi\theta) = Y^T Y - \theta^T \Phi^T Y - Y^T \Phi\theta + \theta^T \Phi^T \Phi\theta. \tag{26}$$

Take the derivative of the objective function and make it zero.

$$\left.\frac{\partial J}{\partial \theta}\right|_{\theta=\hat{\theta}} = -2\Phi^T Y + 2\Phi^T \Phi\hat{\theta} = 0. \tag{27}$$

Thus, it is possible to obtain

$$\Phi^T \Phi\hat{\theta} = \Phi^T Y. \tag{28}$$

Thus, the parameter estimation $\hat{\theta}$, which minimizes the objective function, can be obtained.

$$\hat{\theta} = \left(\Phi^T \Phi\right)^{-1}\Phi^T Y. \tag{29}$$

This result is called the LSE of θ. This method is used in the follow-up generator mathematical model and built-in model calculation.

3. The Structure and Mathematical Model of PCS

The thermal power plant production process is shown in Figure 3. A boiler combined with a steam turbine and a generator constitutes the main equipment of thermal generating units. In order to establish a PCS model of the thermal power unit, a demand assessment should first be carried out clearly to clarify the purpose of modeling. During modeling, it should be noted that models should include only information related to modeling purposes, while other irrelevant information or less relevant information should be discarded or simplified. When verifying the performance of unit PFM, information about the boiler side can be greatly simplified. If the precision of the model requirement is not very high, boiler side characteristics cannot be considered. Therefore, the PCS in the blue square is studied, and its mathematical model will be established for simulation research.
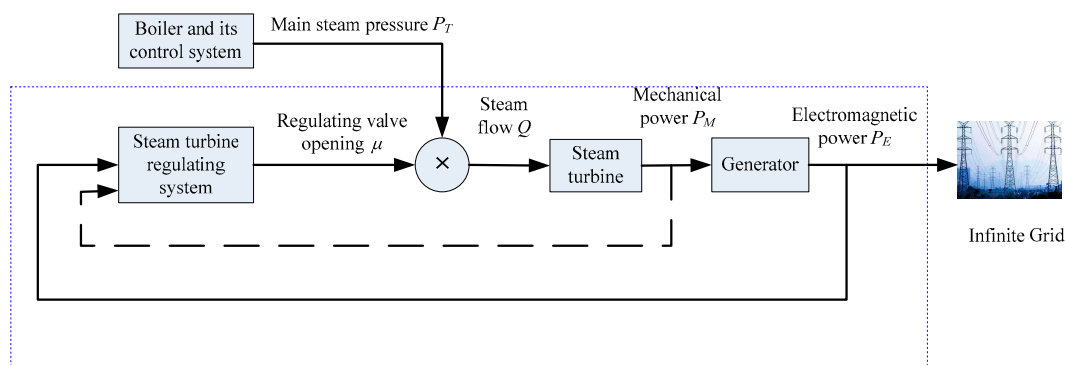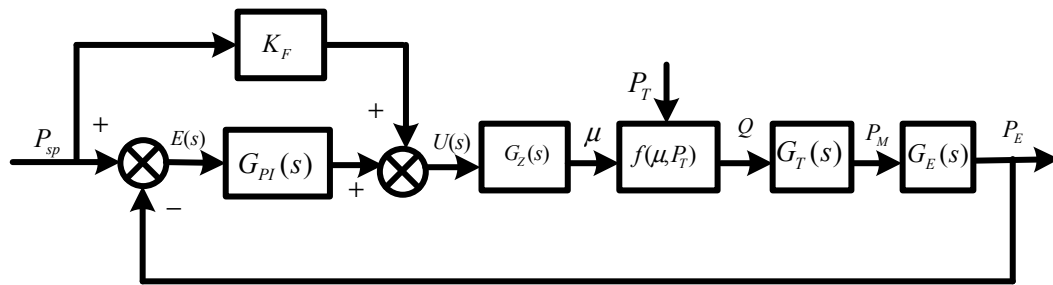

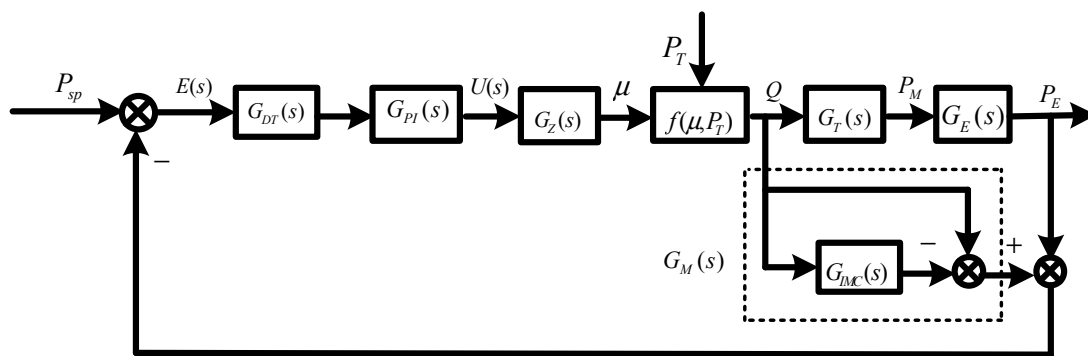**Figure 3.** Production flow chart of the thermal power unit.

3.1. The Structure of the Power Control System

Figure 4 is a typical schematic diagram of a traditional PCS. The control system adopts feed forward (FF) and feedback control, the controlled variable is electromagnetic power P_E, and the reference P_{sp} can be manually set or can be an AGC (automatic generation control) target value. It's just that the power is set in a different way. The sum of the set value and the FM increment is the final power value of FF and feedback control, and the deviation of the electric power are compared with the set value to form a total valve position command so as to control the opening of the steam valve. The opening of the actuator and the main steam pressure determine the steam flow into the turbine, which is expressed by $Q = f(\mu, P_T)$. The steam expands to be mechanical power, and the generator converts it into electromagnetic power pouring into the power grid.
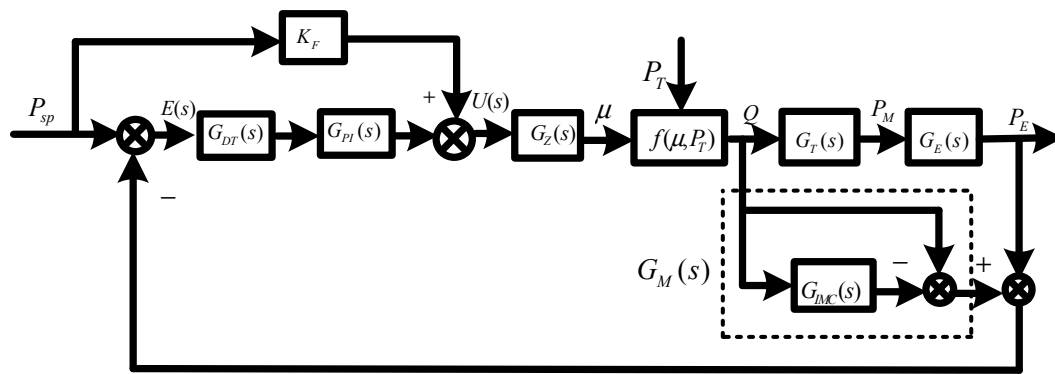

Figure 4. Schematic diagram of power control system (PCS) based on proportional integral (PI) plus feed forward (FF) (P_{sp}—power reference value; $E(s)$—error; $U(s)$—controller output; μ—valve opening; P_T—main steam pressure; Q—steam flow; P_M—mechanical power; P_E—electromagnetic power; K_F—FF gain; $G_{PI}(s)$—controller; $G_Z(s)$—actuator; $f(\mu,P_T)$—function; $G_T(s)$—steam turbine; $G_E(s)$—generator).

Compared with the typical PI plus FF in Figure 4, the structure of PCS based on IMC plus PI is illustrated in Figure 5. The FF function is removed, and the closed loop controller still uses the PI controller. $G_{DT}(s)$ is a mathematical model of the low pass filter, and $G_T(s)$ is the transfer function between Q and P_M, which represents the dynamic relationship between the two variables. The full built-in model $G_M(s) = 1 - G_{IMC}(s)$. The role of $G_M(s)$ is to make the controller work in advance based on the steam flow into the turbine to reflect changes to the input of the controller.

Figure 5. Schematic diagram of the power control system (PCS) based on IMC-PI ($G_{DT}(s)$—low pass filter; $G_M(s)$—built-in model; $G_{IMC}(s)$—transfer function of Q and P_M. (the remaining components are the same as in Figure 4)).

For comparison with Figures 4 and 5, the PCS combines IMC with PI and FF, as shown in Figure 6.

Figure 6. Schematic diagram of PCS based on IMC-PI plus FF. (Please refer to the corresponding components in Figures 4 and 5).

3.2. Mathematical Model of PCS

First in order to carry out the simulation research on the PCS, the mathematical model of each component should be established. Therefore, in this section, the model and the parameters of each component in Figures 4–6, respectively, are determined.

In many cases, the PID can change control strategy easily and flexibly, and the P, PI, PD (Proportion Differentiation), or PID are typical structural composition. The PI control structure is used in this paper.

$$G_{PI}(s) = \frac{U(s)}{E(s)} = K_P + \frac{K_I}{s}. \tag{30}$$

The controller parameters under the two control modes are shown in Table 1.

Table 1. The controller parameters under two control modes (PI: Proportion Integration; FF: Feed forward; IMC: Internal model control).

PI + FF	IMC + PI
$G_{PI1}(s) = 0.20 + \frac{0.05}{s}$ $K_F = 1$	$G_{PI2}(s) = 0.50 + \frac{1}{s}$ $G_{DT}(s) = \frac{1}{2s+1}$ [#] $G_M(s) = 1 - G_{IMC}(s) = 1 - \frac{5.4064s+1}{10.4s+1}$ [##]

Note. [#]: According to the Equation (7) in Section 2.2; [##]: According to the LSE (Least square estimation) method introduced in Section 2.3, $G_{IMC}(s) = \frac{P_m^*}{Q^*} = \frac{T_m s+1}{T_n s+1}$ is determined, where T_m and T_n are parameters to be identified.

The following is the establishment mathematical model of the controlled object, which is the steam turbine and generator [34] of the PCS. The traditional steam turbine governing system model can be applied to most large steam turbine units and the transfer function is as follows.

The electro-hydraulic servo actuator model is

$$G_Z(s) = \frac{\frac{(K_{P1}+\frac{K_{I1}}{s})}{T \cdot s}}{1 + \frac{(K_{P1}+\frac{K_{I1}}{s})}{T \cdot s}}. \tag{31}$$

The turbine model is

$$G_T(s) = \frac{F_{HP} \cdot (1+\lambda) \cdot T_{RH} \cdot s + 1 - F_{LP}}{(T_{CH} \cdot s + 1) \cdot (T_{RH} \cdot s + 1)} + \frac{F_{LP}}{(T_{CH} \cdot s + 1) \cdot (T_{RH} \cdot s + 1) \cdot (T_{CO} \cdot s + 1)}. \tag{32}$$

The definitions and values of all parameters in Equations (31) and (32) are shown in Appendix A.

The parameters in Table A1 (Appendix A) are substituted into Equations (31) and (32), respectively, and the following models are gained.

The actuator model is

$$G_Z(s) = \frac{12s + 1}{0.889s^2 + 12s + 1}. \tag{33}$$

The turbine model is

$$G_T(s) = \frac{5.4064s + 1}{0.52s^2 + 10.45s + 1}. \tag{34}$$

The equivalent forward transfer function of the PCS is

$$G_T^*(s) = G_{PI}(s) \cdot G_Z(s) \cdot G_T(s). \tag{35}$$

Suppose the steam flow into the turbine is a per-unit value

$$Q^* = f(\mu, P_T) = \mu \times P_T^*. \tag{36}$$

In Equation (36), μ is the opening of the electro-hydraulic servo system, and P_T^* is the unitary value of the main steam pressure. When the steam pressure is constant, the relationship between Q^* and μ is linear. Therefore, the definition of the local valve flow coefficient is

$$k = \frac{\Delta Q}{\Delta \mu}. \tag{37}$$

In Equation (37), ΔQ represents the steady-state increment of the actual flow and $\Delta \mu$ represents the steady-state increment of the total valve position.

The main difference between different synchronous generator mathematical models lies in the rotor windings number of motor. If each rotor has two windings, and each rotor windings correspond to the first order differential equations on the d and q axes, then it is called a fourth-order model. Along with the second-order rotor motion equations, the whole generator equations are sixth-order models described in Appendix B (Equations (A1)–(A6)). For the specific parameters and significance, refer to [35,36].

In an actual generator system, if we consider the influence of the excitation system and the power system stabilizer, the generator model will become more complicated because of a high degree of nonlinearity. Therefore, the reduced order model can be used instead of the full order model to ensure that the power simulation response curve is undistorted.

According to the ideas foundation of Prony assessment [37,38], the lower-order model can be extracted from the full order model to obtain the related transfer function by means of the relationship between the output and the input under disturbance. The two parameters measured are the input mechanical power and the output electromagnetic power of the generator. The model can be represented by a second order transfer function expressed by Equation (38) [39]. According to the least square system identification method introduced in Section 2.3, two undetermined parameters of the generator are identified.

$$G_{EN}(s) = \frac{1}{a_1 s^2 + a_2 s + 1}. \tag{38}$$

According to the relationship between the input and output of the generator model, the linear low order model is extracted from the high order model of the generator. The optimization algorithm for system identification is the simplex method, and identified parameters are shown as Equation (39).

$$G_{EN}(s) = \frac{1}{0.0177s^2 + 0.0333s + 1}. \tag{39}$$

Appendix B represents the actual complicated model, and Equation (39) represents a simplified reduced model, and the simulation step response results are shown in Figure 7.
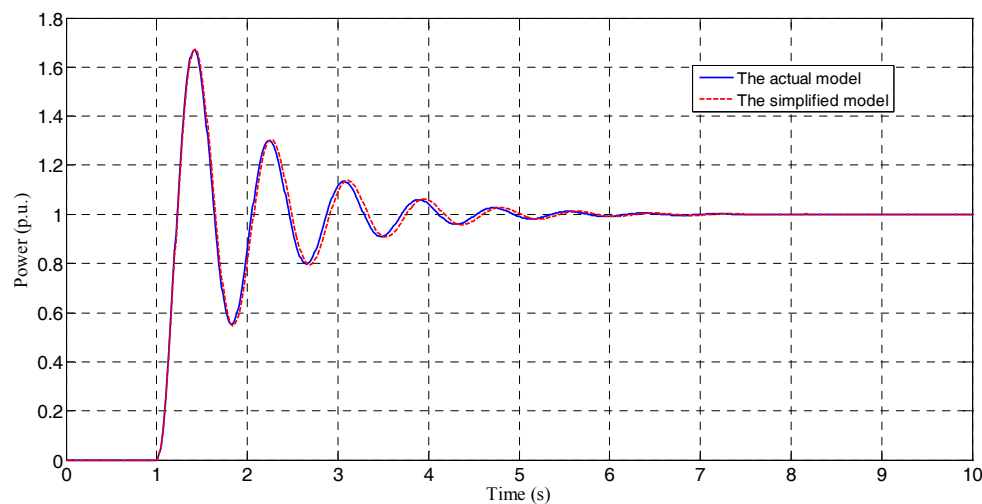
Figure 7. Generator power responses of the actual model and a simplified model.

From Figure 7, it shows that the simplified model can reflect the power response characteristic of the actual model with high accuracy. Since the response curves of the low order model and the high order model coincide well, it is feasible to replace the complex nonlinear model with a low order model.

4. Performance Assessment and Simulation of the Power Control System

In this section, the performance assessment index of the PCS is established first, and further simulation research is then described on the basis of the establishment of each component of PCS in Section 3.
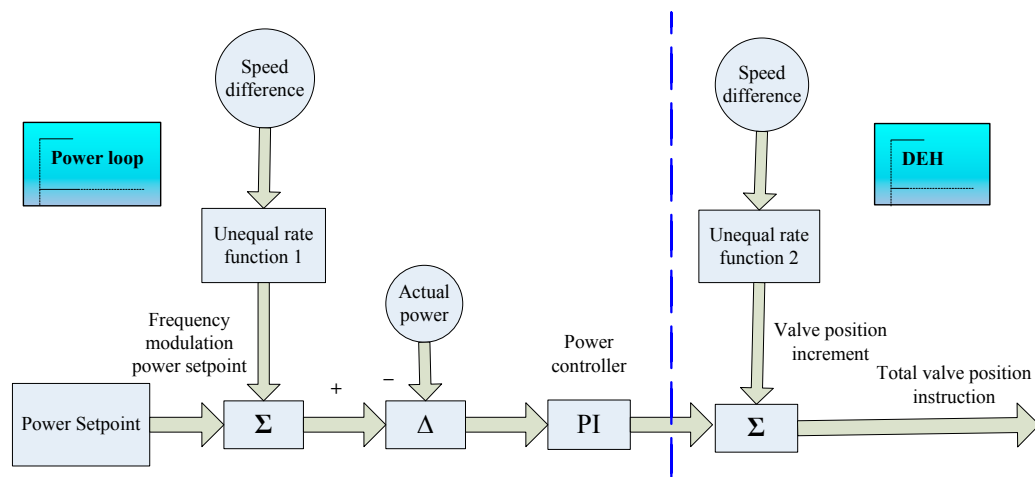
4.1. Dynamic Performance Indexes and Performance Assessment Definition
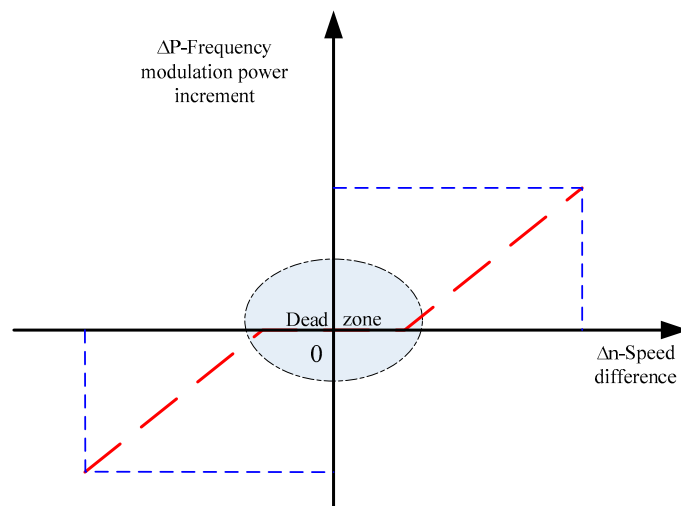
4.1.1. Dynamic Performance Indexes of PCS

A typical schematic diagram of PFM of thermal power unit is shown in Figure 8. The initial FM power constant value is obtained by calculating the speed difference in unit speed through an unequal ratio function (Figure 9). Theoretically, the relation between the actual rotational speed and the frequency of the power grid is $n = 60f$ (r/min). On the side of the power loop, the speed difference which reflects the change of network frequency is compensated by FM power constant value by designing the function of the speed varying rate. The DEH (digital electric hydraulic control system) side makes the rotation speed difference signal directly superimposed on the steam turbine regulator via the rotational speed varying rate design function. On the DEH side, FM directly controls the valve opening regulation of the steam turbine, thereby rapidly changing the unit power. After adjusting the FM effect of the power loop side, closed loop regulation is carried out to ensure steady power and FM target power suppression.

The PFM performance of thermal power units is very important to ensure the frequency stability of the power grid. The control characteristics and operating characteristics of the units have a great influence on the performance of the PFM, so the factors affecting the performance are analyzed below.
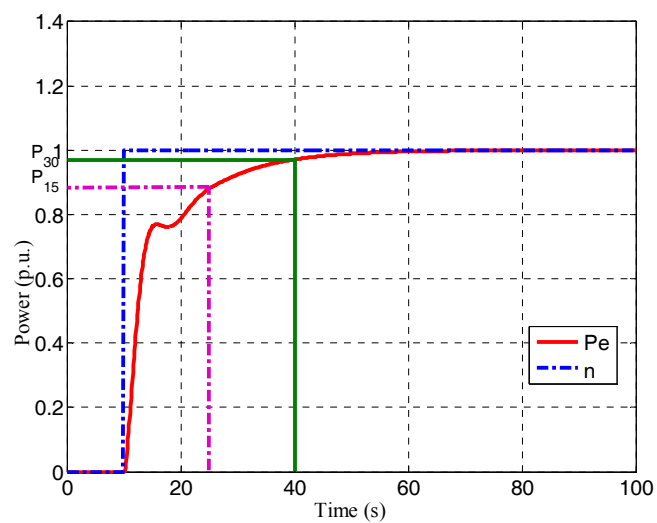
First, the specific indicators for evaluating the performance of primary frequency regulation are confirmed, so three dynamic indicators are selected as part of the performance assessment index according to [40]. The first dynamic index is described as the load time of the coal-fired units. Seventy-five percent of the target load should be less than 15 s. The second dynamic index is described as the load time. A 90% target load should be less than 30 seconds. The third dynamic index is that the stability time of the unit participating in PFM and is less than 1 min. According to Figure 10, the meaning of the three dynamic indexes is explained below.

Figure 8. Typical schematic diagram of primary frequency modulation (PFM) of thermal power unit (DEH: Digital Electro-hydraulic Control).

Figure 9. Rotational speed inequality curve.

Figure 10. Typical power response curve.

Under a simulation environment, turbine speed step change is artificially simulated, and the the PFM loop quickly changes the turbine mechanical output power, so power response characteristics

of the unit can be obtained under frequency disturbance. As shown in Figure 10, when the unit speed signal has a step change n and the speed discrepancy exceeds the death zone (e.g., ±2 r/min) in Figure 10, then the unit's frequency function begins to change the power of the unit. The time of the step change of the speed signal is the starting time of the PFM action. The symbol P_e means the power change, and the power of the unit reaches a steady value of P_{sp} as the action of PFM continues. After PFM action lasts 15 s, according to the requirements of the first dynamic, the variation of power $P_{15}/P_{sp} \times 100\%$ should be greater than 75%. When the PFM action continues for 30 s, according to the second dynamic index, the variation of power $P_{30}/P_{sp} \times 100\%$ should be greater than 90%. According to the third dynamic index, the stable time of PFM action should be less than 60 s.

The PFM performance assessment indicators are defined as follows.

$$\beta_1 = \frac{P_{15}}{P_{sp}}. \tag{40}$$

$$\beta_2 = \frac{P_{30}}{P_{sp}}. \tag{41}$$

$$t_S(\Delta = \pm 2\%). \tag{42}$$

In Equation (17), t_S is the adjustment time of the PFM and the error band is marked as $\Delta = \pm 2\%$.

In order to evaluate the performance of the PFM, the power grid dispatching has the corresponding means to assess. Taking the Hunan Province power grid in China as an example, the implementation of the assessment of PFM of thermal power units is according to the related requirements of two documents [41,42]. In these two detailed sets of rules, the main basis for the assessment of PFM is the unit contribution rate, which is defined as

$$\left. \begin{array}{l} K = \frac{H_i}{H_e} \times 100\% \\ H_i = \int_{t_0}^{t_1} (P_t - P_0)dt \\ H_e = \int_{t_0}^{t_1} \Delta P(\Delta f, t)dt \end{array} \right\}. \tag{43}$$

In Equation (43), K is a power PFM contribution rate that represents the percentage of the real contribution H_i and the theoretical contribution H_e. The actual contribution H_i represents the integral value of the actual power variation. The theoretical contribution H_e represents the integral value of the theoretical FM power variation calculated according to the unequal speed rate in the FM duration. If $K < 50\%$, the PFM of the unit will be considered unqualified. On the contrary, it will be considered qualified.

According to Equations (40)–(43), the chosen performance assessment indexes of PCS include a total of four items as shown in Table 2.

Table 2. Dynamic performance indexes and qualified scope of the power control system (PCS).

Performance Dynamic Index	Qualified Scope
β_1 (%)	≥ 75%
β_2 (%)	≥ 90%
t_S (s)	≤ 60s
K(%)	≥ 50%

4.1.2. Dynamic Performance Assessment Index Definition of PCS

Definition: The dynamic performance assessment index of PFM for PCS *DPAI* (Dynamic Performance Assessment Index) as

$$\begin{cases} DPAI = \lambda_1 \frac{\beta_1}{0.75} + \lambda_2 \frac{\beta_2}{0.90} + \lambda_3 \frac{60}{t_s} + \lambda_4 \frac{K}{0.50} \\ \lambda_1 + \lambda_2 + \lambda_3 + \lambda_4 = 1 \\ \text{And} \quad \beta_1 \geq 75\%, \ \beta_2 \geq 90\%, t_s \leq 60s, K \geq 50\% \end{cases} . \tag{44}$$

At the same time, another auxiliary performance assessment index Num is given, i.e., the number of dynamic performance indicators satisfying the eligible range of parameters in Table 2. The same weights for four dynamic performance metrics are given.

$$\lambda_1 = \lambda_2 = \lambda_3 = \lambda_4 = 0.25. \tag{45}$$

Finally, the performance assessment benchmarks and results for the PCS are shown in Table 3 below.

Table 3. Benchmark and result of dynamic performance assessment for the PCS (*DPAI*: Dynamic Performance Assessment Index).

DPAI	**Num**	**Performance Assessment Results**
$DPAI \geq 1.4$	Num = 4	Excellent
$1.4 > DPAI \geq 1.3$	$3 \leq \text{Num} \leq 4$	Good
$1.3 > DPAI \geq 1.0$	$2 \leq \text{Num} \leq 4$	Medium
$1.0 > DPAI \geq 0.5$	1	Poor
$0.5 > DPAI > 0$	0	So Bad
System Unstable	0	Unacceptable

The structure of PCS shown in Figures 4–6 are, respectively, adopted below. According to the established mathematical model in Section 3.2 and the performance assessment indexes as the benchmark in Table 3, a deep assessment of the specific factors affecting PFM was carried out under the MATLAB (Version: 8.0.0.783(R2012b), MathWorks, Natick, MA, USA, 2017) simulation environment.

The simulation software version is Matlab2012b and the simulation and performance assessment flow is as follows: (1) build the simulation model; (2) calculate the four dynamic performance indexes; (3) calculate the main and auxiliary performance assessment indexes. The result is given depending on the circumstances.

4.2. Simulation of PCS

It is assumed that all equipment in the PCS works in the rated condition, and the disturbance signal is applied to it at the stable state. In this way, the mathematical model of each part can be simplified in the form of transfer function, which is convenient to establish the simulation model of the PCS in the MATLAB environment. Corresponding to the control structures of Figures 4–6, the simulation model of the controlled object is established, respectively, using Equations (33), (34), and (39). Using the proper tuning method of controller parameters and selecting suitable parameters, the dynamic performance of PCS was analyzed. In order to obtain an ideal control effect, the controller needs features that match with the controlled object. Because the dynamic characteristics cannot be easily changed, only reasonable controller parameters can be set. In engineering, commonly used parameter tuning methods include the critical proportional band method, the attenuation curve method, the dynamic parameter method, and the empirical method [43–45]. The critical proportional zone method has certain limitation in practical applications. Some production processes do not allow for the generation of other side oscillations such as boiler drum level control in thermal power plants, and some controlled objects with larger inertia do not easily generate equal amplitude oscillations, so the proportional band and oscillation period cannot be obtained under critical conditions. The attenuation curve method was developed based on the critical proportional band method and has similar limitations. The dynamic parameter method requires the system to be tested with a step disturbance test under an open loop condition. Parameters are calculated according to the step response curve. The empirical method
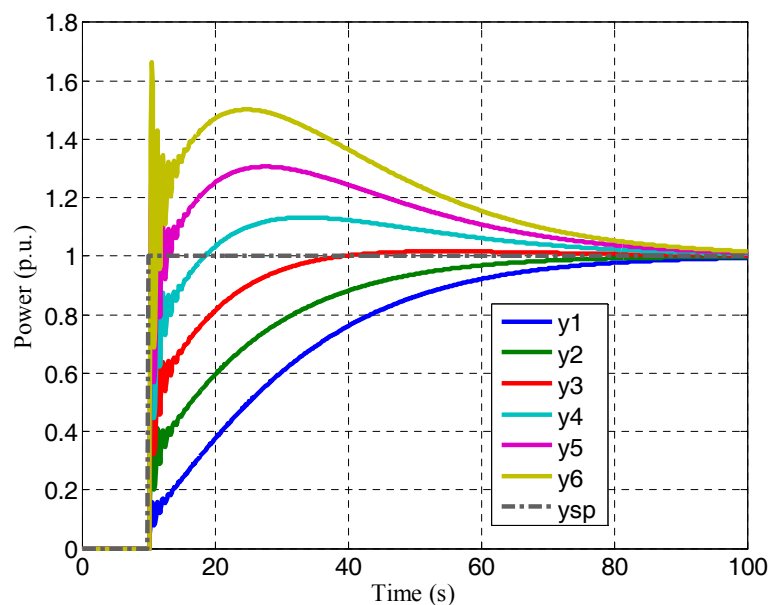
is essentially a method of trial and error. It is an effective method that is summed up in production practice and widely applied in process control field. The steps of this method are described according to operational experience. A set of controller parameters is determined, and closed loop operation is performed. Step disturbance is then added to observe the adjustment process. If the adjustment process is unsatisfactory, regulator parameters are modified, and the disturbance test is repeated until the adjustment process is satisfactory. Finally, the combination of the empirical method and the theoretical algorithm introduced in Section 2.2 is used in this paper, so the performance differences can be compared directly under different parameters during parameter tuning.

The influence of the different control parameter on the control effect is complex and profound. Therefore, how to achieve the best PFM effect requires analysis of the relationship between different control parameters and PFM performance. For the stability and security requirements of the actual PCS, the conditions for comprehensive analytical research are not available, so the simulation of PCS was carried out under the following four cases. Suppose the local flow characteristic coefficient $k = 1$ in Equation (37).

4.2.1. The Influence of FF Coefficient K_F on PCS

Firstly, the influence of FF coefficient on PFM was analyzed. In Figure 4, through the total valve position instructions, the comprehensive valve position increment directly controls the steam turbine regulating valve and plays a fast regulation role. The PFM is a kind of disturbance for the stable operation of the unit since it changes power of the assembling unit quickly. In order to better balance the PFM and the stable operation of the unit, the comprehensive increment of the valve position is not directly superimposed on the total valve position instruction, instead adjusted by FF gain coefficient and then apply to it. Changing K_F can adjust the primary frequency disturbance degree.

Let $K_F = 0/0.4/0.8/1.2/1.6/2.0$, and the controller is $G_{PI}(s) = 0.2 + \frac{0.05}{s}$. The power simulation curve of the PFM test is shown in Figure 11.

Figure 11. The response of PCS with different FF coefficients.

According to the power curve shown in Figure 8, β_1, β_2, t_S, and K are calculated, respectively, when $K_F = 0/0.4/0.8/1.2/1.6/2.0$. The results are shown in Table 4.

According to the requirements of β_1, β_2, t_S, and K, Table 4 shows that β_1, β_2, and K increase to obtain better performance with the increase of K_F, but the effect of K_F on t_S is not monotonic; that is, a K_F value that is too small or too big will increase t_S. Therefore, to make t_S qualified, K_F should be

selected in the appropriate range. For K_F, we ensure that a larger value is selected to optimize the performance of PFM on the premise that t_S is qualified.

Because K_F is not the only factor that affects the performance of PFM, the influence of different power controller parameters on their performance is further studied below.

Table 4. Performance result of primary frequency modulation (PFM) with different controllers.

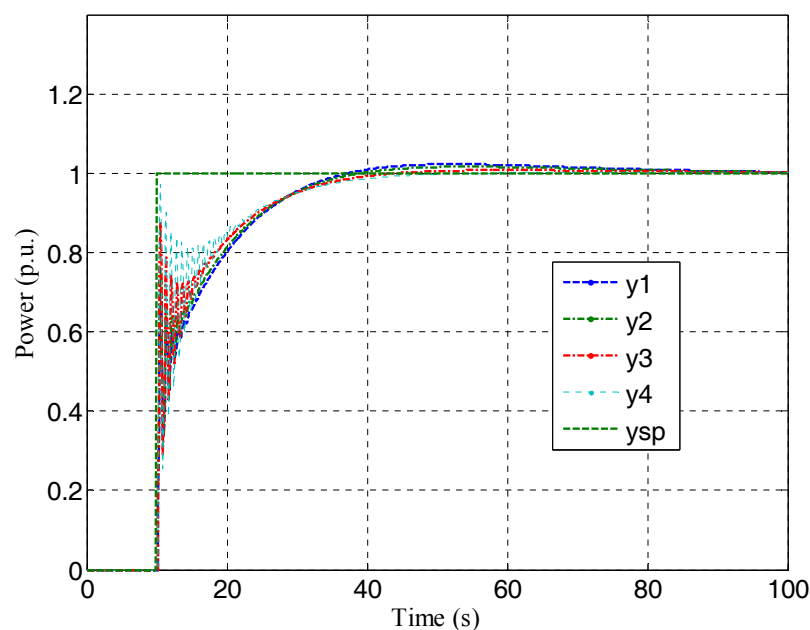| K_F	Output	β_1 (%)	β_2 (%)	t_S (s)	K(%)	*DPAI*	Num	Performance
0	y1	49.52	75.88	72.10	70.08	0.9232	1	Poor
0.4	y2	69.66	88.05	56.50	78.02	1.1195	2	Medium
0.8	y3	89.79	100.22	24.20	85.95	1.6126	4	Excellent
1.2	y4	109.93	112.39	72.80	93.88	1.3376	3	Good
1.6	y5	130.06	124.56	81.50	101.80	1.4544	3	Good
2.0	y6	150.20	136.73	86.80	109.80	1.5823	3	Good

4.2.2. Influence of Controller Parameters on PCS

The PI control strategy is usually adopted in the power controller of the actual unit. When the parameter setting of the PI controller is not reasonable, the PFM performance of the unit will be decreased. According to Section 4.2.1 and the results in Table 3 and Figure 11, the FF coefficient performs best when it is 0.8, so it may be assumed that it is 0.8. Therefore, let $K_F = 0.8$, keep the PI integral gain $K_I = 0.05$, and change the PI proportional gain. Four different power controllers are shown in Table 5.

Table 5. Performance results of PFM with different controllers.

Controller	Output	β_1 (%)	β_2 (%)	t_S (s)	K(%)	*DPAI*	Num	Performance
$G_{c1}(s) = 0.10 + 0.05/s$	y1	89.40	100.88	50.80	85.96	1.2885	4	Medium
$G_{c2}(s) = 0.20 + 0.05/s$	y2	89.79	100.22	24.20	85.95	1.6126	4	Excellent
$G_{c3}(s) = 0.40 + 0.05/s$	y3	90.51	99.25	25.80	85.95	1.5740	4	Excellent
$G_{c4}(s) = 0.60 + 0.05/s$	y4	90.97	98.61	27.40	85.97	1.5400	4	Excellent

The power simulation curve with different proportional gain is shown in Figure 12, and the results of four performance indexes are also shown in Table 5.

Figure 12. PCS response with different proportional gain.

When $K_P = 0.95$, the system becomes unstable and the output power oscillates as shown in Figure 13. It can be seen from Figure 13, if the proportional gain becomes larger, the stability of the system will decline.
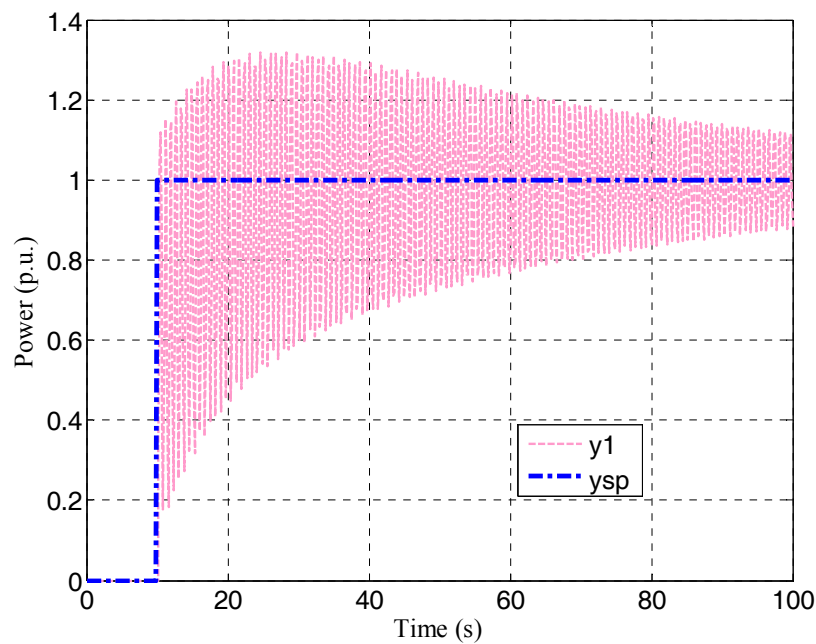

Figure 13. Oscillatory output of PCS.

As can be seen in Table 5, the performance of $G_{c2}(s) = 0.20 + 0.05/s$ is superior, so the proportional gain $K_P = 0.20$ is kept unchanged. The PI integral gain is then changed, and six different power controllers are compared with each other. The power simulation curve with different integral gain is shown in Figure 14, and the results of four performance indexes are shown in Table 6.
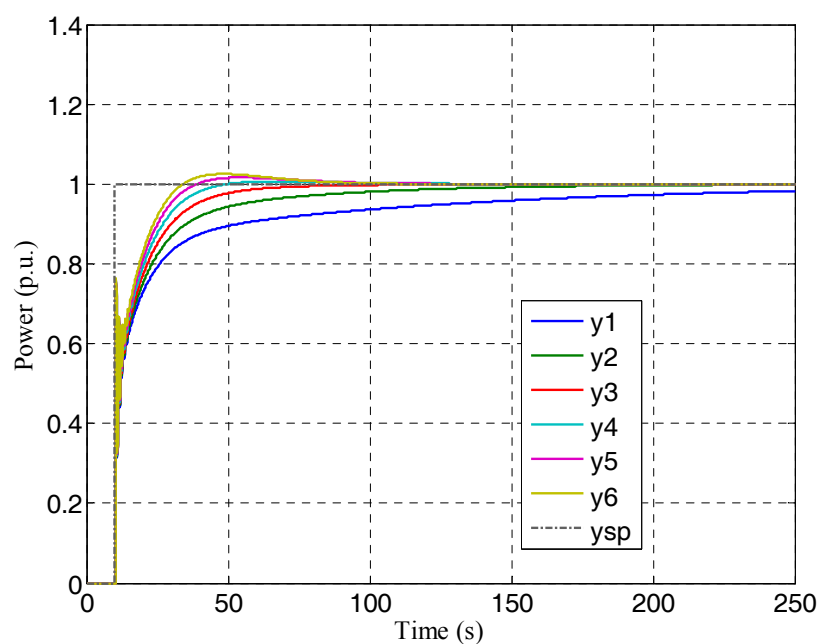

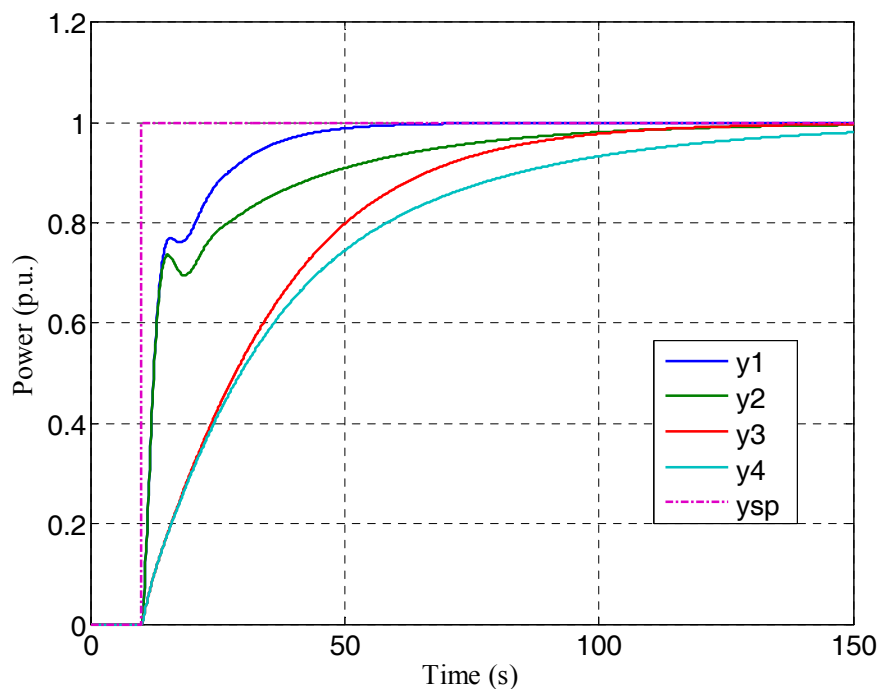**Figure 14.** PCS response with different integral gains.

Table 6. Performance result of PFM with different controllers.

Controller	Output	β_1 (%)	β_2 (%)	t_S (s)	K(%)	*DPAI*	Num	Performance
$G_{c1}(s) = 0.20 + 0.01/s$	y1	79.11	87.37	223.80	77.37	0.9475	1	Poor
$G_{c2}(s) = 0.20 + 0.02/s$	y2	82.18	91.83	88.30	81.06	1.0908	3	Medium
$G_{c3}(s) = 0.20 + 0.03/s$	y3	84.96	95.35	42.30	83.41	1.3058	4	Good
$G_{c4}(s) = 0.20 + 0.04/s$	y4	87.49	98.10	29.70	84.94	1.4795	4	Good
$G_{c5}(s) = 0.20 + 0.05/s$	y5	89.79	100.22	24.20	85.95	1.6126	4	Excellent
$G_{c6}(s) = 0.20 + 0.06/s$	y6	91.87	101.82	49.70	86.65	1.3399	4	Good

The simulation results in Figure 14 show that a reasonable setting of control parameters is very important for PFM. When $K_I = 0.01$, under the action of the integral element, power changes to the target value at a slower speed, but when $G_{c5}(s) = 0.2 + 0.05/s$, the $G_c(s)$ control parameter setting is more reasonable, and the power response characteristics are more ideal, so the power reaches the target value in a relatively short period of time. The simulation results show that the control parameters affect the steady state response characteristics of the PCS, so the reasonable control parameter setting is important to ensure t_S, which is on behalf of the steady state performance of qualified PFM.

4.2.3. Simulation Study of IMC-PI PCS

The IMC-PI structure in Figure 5 was adopted, and two parameters of built-in model and two different parameters of PI controller were selected individually. The results of the comparison under four different cases are shown in Figure 15, and the results of four performance indexes are shown in Table 7.

Figure 15. PCS response with four different IMC-PI parameters.

From Figure 15 and Table 7, we can see that the performance of the system is getting worse under the four different parameters. This means that the performance of the system under the first parameter is the best. The best parameter is also used in Section 4.2.4 below.
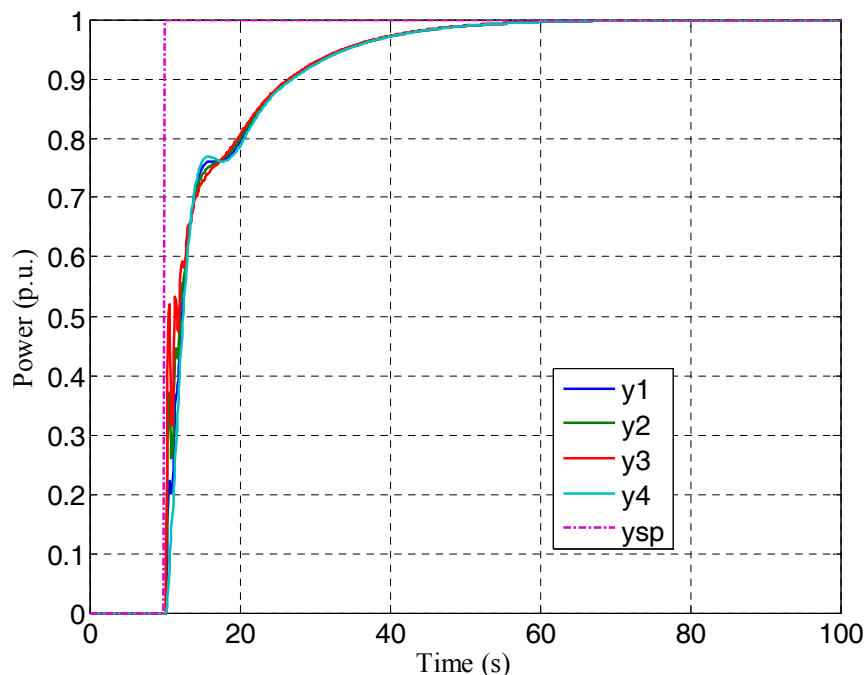
Table 7. Performance result of PFM with four different controllers.

Controller			Output	β_1 (%)	β_2 (%)	t_S (s)	K(%)	DPAI	Num	Performance
$G_c(s) = 0.50 + \frac{1}{s}$	$G_{IMC}(s) = \frac{5.4064s+1}{10.40s+1}$	#	y1	87.83	97.08	33.90	84.01	1.4108	4	Good
$G_c(s) = 0.50 + \frac{1}{s}$	$G_{IMC}(s) = \frac{11.90s+1}{22.80s+1}$	#	y2	78.28	87.40	87.80	78.69	1.0552	2	Poor
$G_c(s) = 0.20 + \frac{0.05}{s}$	$G_{IMC}(s) = \frac{5.4064s+1}{10.40s+1}$	#	y3	42.56	68.81	92.00	65.49	0.8134	1	Poor
$G_c(s) = 0.20 + \frac{0.05}{s}$	$G_{IMC}(s) = \frac{11.90s+1}{22.80s+1}$	#	y4	41.27	64.84	138.00	61.75	0.7256	1	Poor

#: According to the LSE system identification method introduced in Section 2.3, $G_{IMC}(s) = \frac{P_m^*}{Q^*} = \frac{T_m s+1}{T_n s+1}$ is determined, where T_m and T_n are parameters to be identified.

4.2.4. PCS Response under IMC-PI Plus FF

The IMC-PI plus the FF structure in Figure 6 was adopted, and the performance of IMC-PI under a different FF coefficient is shown in Figure 16. The performance index of PFM is shown in Table 8.

Figure 16. The power response of IMC-PI plus different FF coefficient.

Table 8. Performance result under IMC-PI with different FF coefficients.

K_F	Output	β_1 (%)	β_2 (%)	t_S (s)	K(%)	DPAI	Num	Performance
0.00	y1	87.83	97.08	33.90	84.01	1.4108	4	Good
0.20	y2	87.99	97.13	33.90	84.21	1.4124	4	Good
0.40	y3	88.15	97.18	33.90	84.41	1.4141	4	Good
0.60	y4	88.30	97.23	33.90	84.61	1.4157	4	Good

Figure 16 and Table 8 show that the four performance indexes of PFM change little with the increase in FF coefficient. Even the oscillation of output power increases, and the stability becomes worse, so FF control is not suitable for IMC.

When choosing the control strategy of the PCS, from the assessment of Sections 4.2.1 and 4.2.2, the performance of the traditional PI controller with FF is better than that without FF, while the performance of IMC without FF is better than that with FF according to the assessment of Sections 4.2.3 and 4.2.4. The main result of Section 4 is that FF control improves the conventional PI control.

The above conclusions are based on the ideal situation that is the local flow coefficient $k = 1$, so its effect on the performance of PCS will be further studied under the following circumstances in Section 5 below.

5. Robustness Assessment of the PI and IMC Control Structures

5.1. Valve Local Flow Coefficient k

When the thermal power unit is connected to the grid, the electro-hydraulic governor usually consists of four or six turbine control valves. There is only one electrical agency in the model that represents all turbine control valves. The valve management of the actual unit has two modes: sequence valve mode and single valve mode. When the unit is in sequence valve mode, the openings of every turbine control valve are not necessarily equal, but when the unit is in single valve mode, the openings of every turbine control valve are equal. The valve characteristic test was carried out on a certain 300 MW unit in sequence valve mode and single valve mode, respectively. During the test, the main steam pressure, the main steam temperature, and the condenser vacuum were kept relatively stable, and the test data are shown in Tables 8 and 9. At the same time, all local flow coefficients were calculated according to Equation (12) and are listed in the rightmost column of Tables 9 and 10.

Table 9. Test data and local valve flow coefficients in sequence valve mode.

Total Opening of Valve-μ(%)	Power-P_E(MW)	Steam Flow-Q(%)	Local Flow Coefficient-k
68.00	184.40	61.47	-
68.60	199.60	66.53	8.433
70.10	255.30	75.10	5.713
72.10	237.00	79.00	1.950
75.10	241.90	80.63	0.543
79.10	247.30	82.43	0.450
81.10	246.40	82.13	−0.150
83.10	247.30	82.43	0.150
87.10	257.70	85.90	0.868
88.50	280.40	93.47	5.407
92.50	284.60	94.87	0.350
97.00	287.20	95.73	0.191
99.00	290.00	96.67	0.470
100.00	294.20	98.07	1.400

Table 10. Test data and local valve flow coefficients in single valve mode.

Total Opening of Valve-μ(%)	Power-P_E(MW)	Steam Flow-Q(%)	Local Flow Coefficient-k
86.00	182.50	60.83	-
87.00	186.00	62.00	1.170
88.00	192.00	64.00	2.000
89.00	198.50	66.17	2.170
90.00	202.80	67.60	1.430
90.50	205.50	68.50	1.800
91.00	209.00	69.67	2.340
91.50	220.20	73.40	7.460
92.00	228.40	76.13	5.460
92.50	242.00	80.67	9.080
93.00	248.90	82.97	4.600
94.00	260.10	86.70	3.730
95.00	265.10	88.37	1.670
96.00	273.80	91.27	2.900
97.00	283.60	94.53	3.260
98.00	286.80	95.60	1.070
100.00	296.10	98.70	1.550

From Table 9, in sequence valve mode, the relationship between μ and Q is shown in Figure 17, and the relationship between μ and P_E is shown in Figure 18.
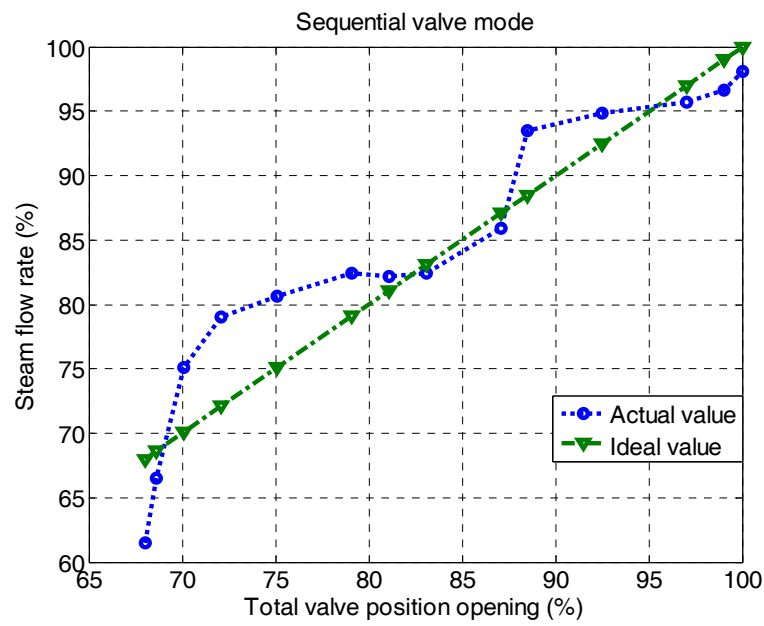
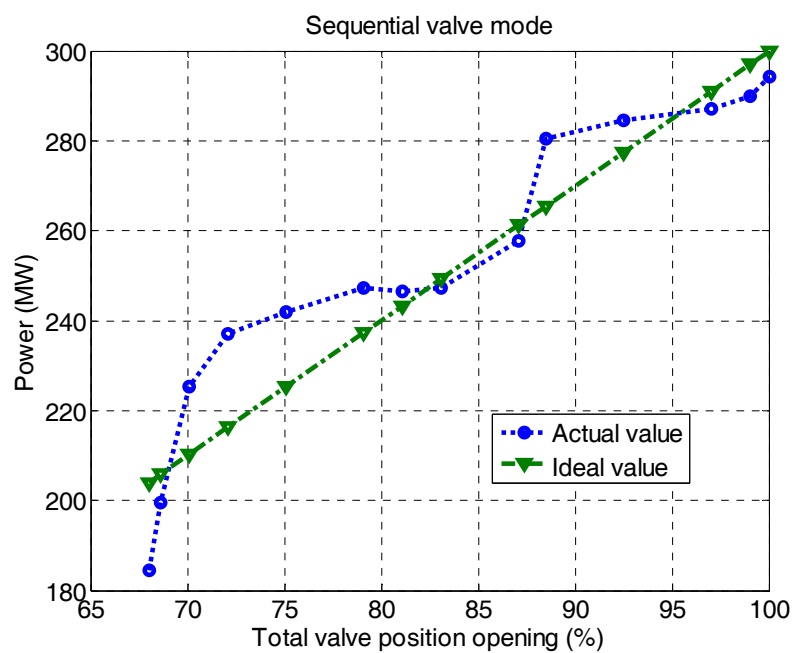**Figure 17.** The relationship between μ and Q.

Figure 18. The relationship between μ and P_E.

From Table 10, in single valve mode, the relationship between μ and Q is shown in Figure 19, and the relationship between μ and P_E is shown in Figure 20.
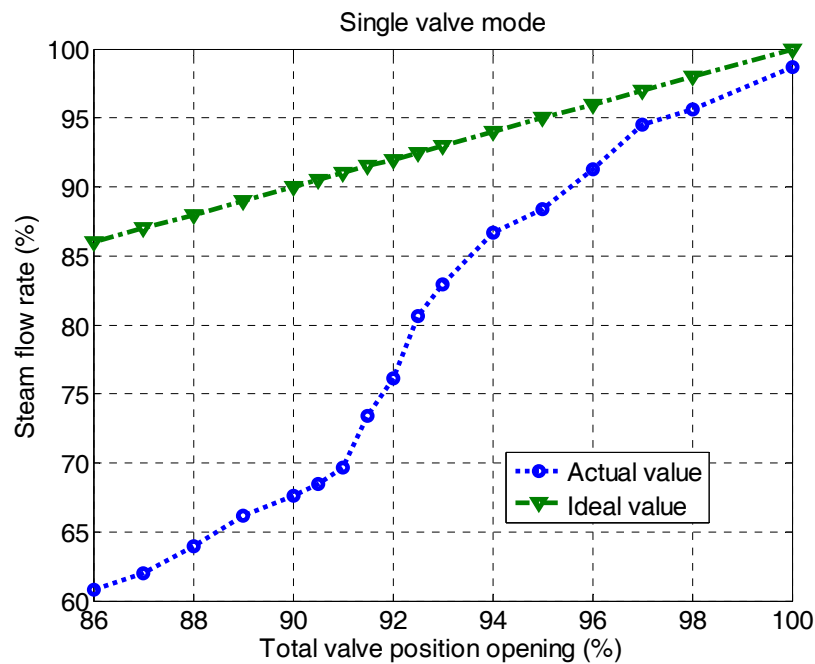
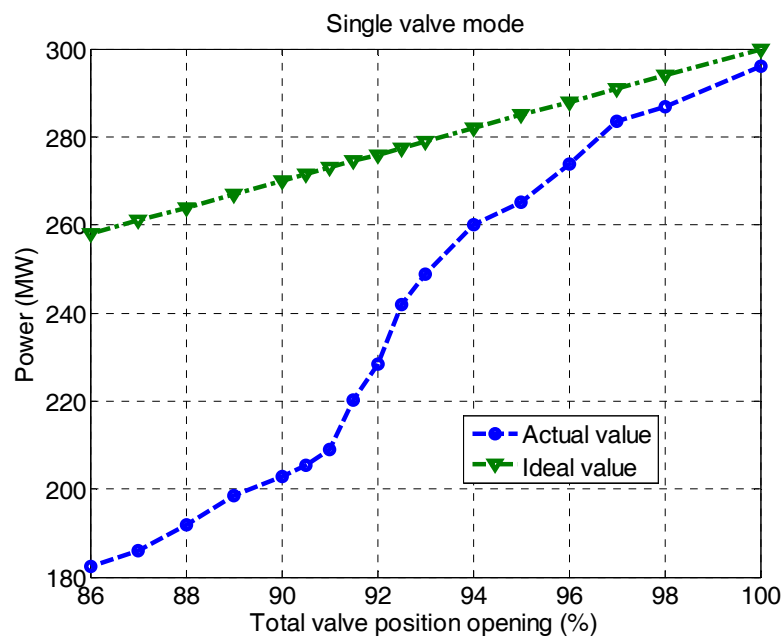**Figure 19.** The relationship between μ and Q.

Figure 20. The relationship between μ and P_E.

From Figures 17 and 19, it can be seen that there is a great deviation between the actual flow curve and the ideal curve of the unit, showing a strong nonlinearity. Similarly from Figures 18 and 20, it can also be seen that there is a great deviation between the actual power curve and the ideal curve of the unit, and this deviation is due to the nonlinear nature of the valve flow characteristics.

In order to quantify the deviation between the actual flow curve and the ideal curve of the unit, the local flow coefficient is used to express the effect of the change of the total valve opening on the steam flow. In sequence valve mode, the relationship between μ and k is shown in Figure 21. In single valve mode, the relationship between μ and k is shown in Figure 22.
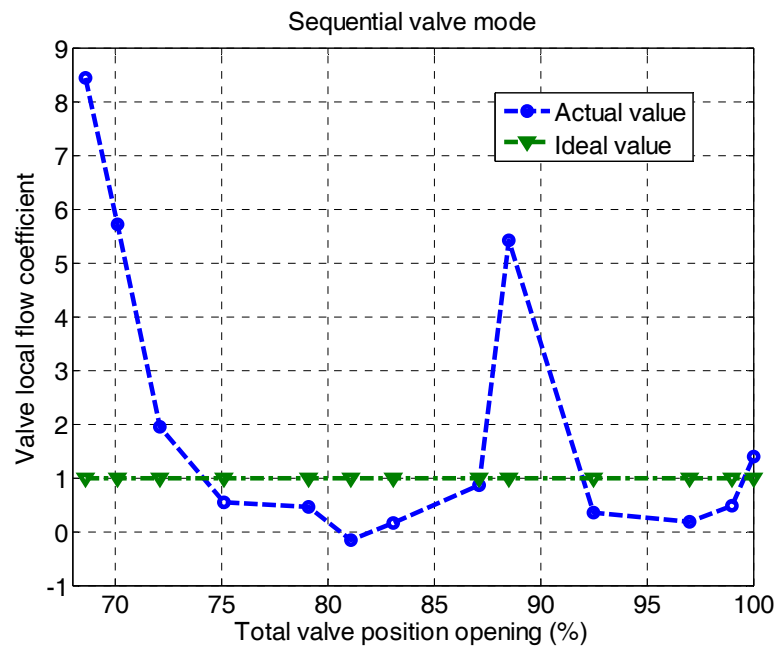
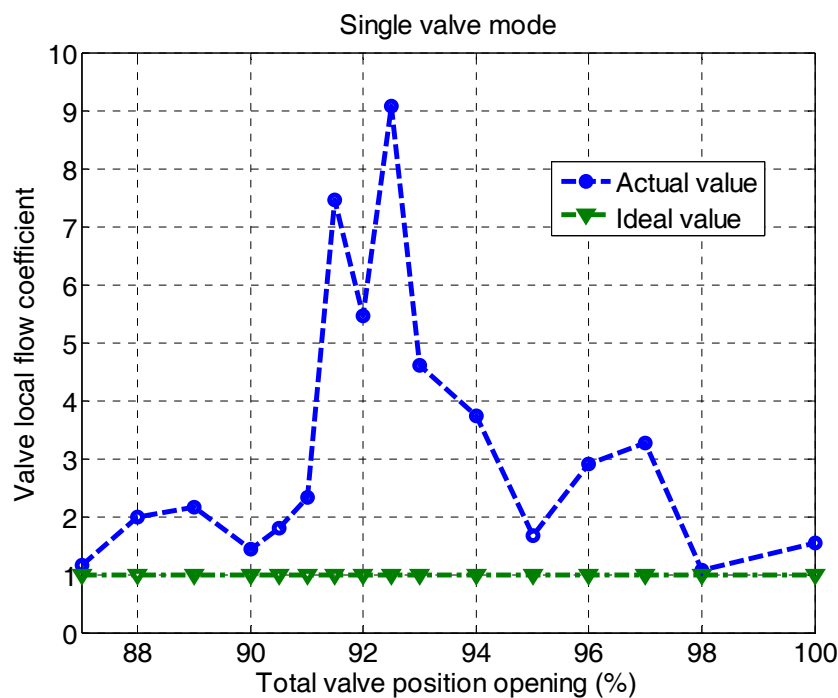**Figure 21.** The relationship between μ and k.

Figure 22. The relationship between μ and k.

5.2. The Influence of k on PCS Performance

In the case of different local flow coefficients, the output y1 of PCS under traditional PI plus FF control, which is compared with the output of y2 under IMC plus PI. In other words, the control structures in Figures 4 and 5 are used to study the effect of valve local flow coefficient on PCS. According to the assessment results of Sections 4.2.1 and 4.2.2, the PI controller $G_{c5}(s) = 0.20 + 0.05/s$ in Table 6 and the FF coefficient $K_F = 0.8$ are adopted. Similarly according to the assessment results of Sections 4.2.3 and 4.2.4, the control parameters $G_{IMC}(s) = \frac{5.4064s+1}{10.40s+1}$ and $G_c(s) = 0.50 + \frac{1}{s}$ in Table 7 are adopted.

When $k \in (0, 1.0]$, the out power under PI plus FF and IMC-PI are shown in Figure 23, and the corresponding performance results are shown in Tables 11 and 12.
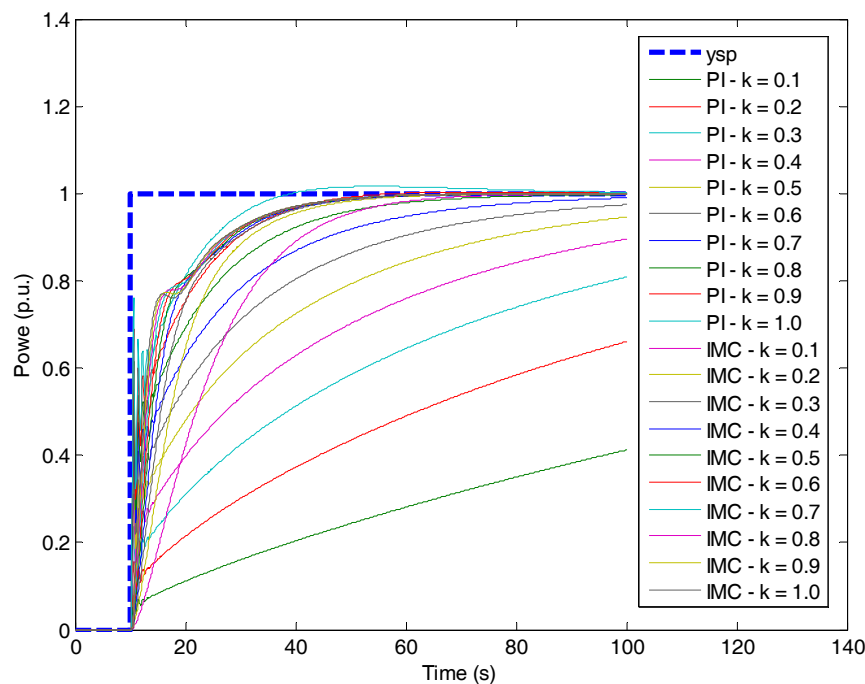

Figure 23. The power response with $k \in (0, 1.0]$.

Table 11. The performance result with $k \in (0, 1.0]$.

k	PI plus FF Control						
	β_1 (%)	β_2 (%)	t_S (s)	K(%)	*DPAI*	Num	Performance
0.10	13.63	20.33	761.70	22.82	0.2327	0	So Bad
0.20	25.93	37.19	369.10	39.47	0.4223	0	So Bad
0.30	37.01	51.18	236.90	51.79	0.5803	1	Poor
0.40	47.02	62.77	169.40	61.01	0.7155	1	Poor
0.50	56.06	72.37	127.40	68.03	0.8352	1	Poor
0.60	64.23	80.30	97.20	73.44	0.9469	1	Poor
0.70	71.61	86.84	72.60	77.67	1.0622	1	Poor
0.80	78.29	92.22	50.80	81.04	1.2041	2	Medium
0.90	84.33	96.62	34.20	83.74	1.3927	4	Good
1.00	89.79	100.22	34.20	85.95	1.4314	4	Excellent

Table 12. The performance result with $k \in (0, 1.0]$.

k	IMC-PI Control						
	β_1 (%)	β_2 (%)	t_S (s)	K(%)	*DPAI*	Num	Performance
0.10	60.75	88.96	49.00	75.01	1.1178	2	Medium
0.20	80.40	95.50	38.50	80.01	1.3090	4	Good
0.30	85.29	96.31	36.30	81.67	1.3593	4	Good
0.40	85.97	96.64	35.40	82.51	1.3772	4	Good
0.50	86.03	96.80	34.90	83.01	1.3864	4	Good
0.60	86.31	96.90	34.60	83.34	1.3929	4	Good
0.70	86.78	96.97	34.30	83.58	1.3997	4	Good
0.80	87.26	97.02	34.20	83.76	1.4036	4	Excellent
0.90	87.62	97.05	34.00	83.90	1.4081	4	Excellent
1.00	87.83	97.08	33.90	84.01	1.4108	4	Excellent

　　　Figure 23, Table 11, and Table 12 show that three indexes are not qualified under $k \in (0, 0.7]$, so the performance of PCS under traditional PI plus FF is very poor. Only when $k \in [0.8, 1.0]$ are all four indexes qualified. As a contrast, all indexes of PCS based on IMC are superior to the traditional one.

　　　Similarly, when $k \in (1.0, 2.0]$, the out power under PI plus FF and IMC-PI are, respectively, shown in Figure 24, and the corresponding performance results are shown in Tables 13 and 14.
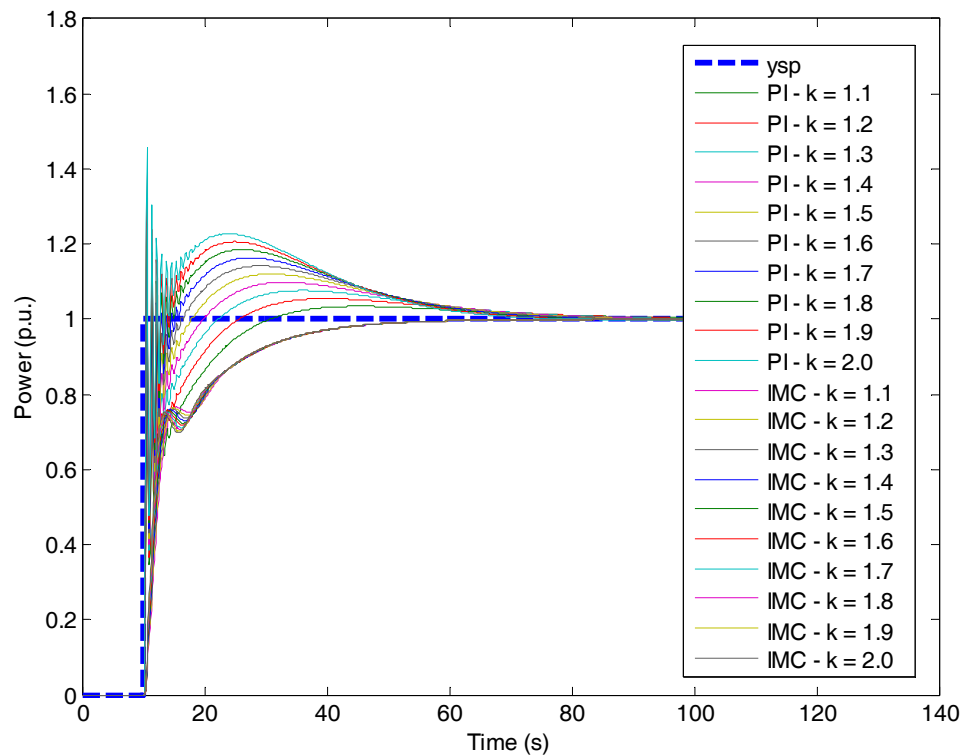

Figure 24. The power response with $k \in (1.0, 2.0]$.

Table 13. The performance result with $k \in (1.0, 2.0]$.

k	PI plus FF Control						
	β_1 (%)	β_2 (%)	t_S (s)	K(%)	*DPAI*	Num	Performance
1.10	94.74	103.14	55.60	87.78	1.2959	4	Good
1.20	99.21	105.49	58.50	89.31	1.3113	4	Good
1.30	103.27	107.36	58.90	90.60	1.3344	4	Good
1.40	106.93	108.84	58.30	91.71	1.3587	4	Good
1.50	110.25	109.99	57.40	92.67	1.3816	4	Good
1.60	113.26	110.86	56.20	93.51	1.4037	4	Excellent
1.70	115.97	111.50	55.00	94.25	1.4240	4	Excellent
1.80	118.43	111.95	53.80	94.90	1.4427	4	Excellent
1.90	120.65	112.25	52.60	95.49	1.4602	4	Excellent
2.00	122.66	112.41	51.40	96.01	1.4766	4	Excellent

　　　Figure 24, Table 13, and Table 14 show that the four performance indexes of PCS, respectively, based on traditional PI and IMC are qualified under $k \in (1.0, 2.0]$. For the three indexes, β_1, β_2, and K, the PI plus FF performance is better than IMC-PI, but for t_S, the IMC is superior to PI plus FF. In a word, the overall performance of IMC-PI is stable and superior to the traditional one.

　　　Similarly, when $k \in (2.0, 16.0)$, the out power under PI plus FF and IMC-PI are, respectively, shown in Figure 25, and the corresponding performance indexes are shown in Tables 15 and 16.

Table 14. The performance result with $k \in (1.0, 2.0]$.

k	IMC-PI Control						
	β_1 (%)	β_2 (%)	t_S (s)	K(%)	DPAI	Num	Performance
1.10	87.93	97.11	33.90	84.10	1.4116	4	Excellent
1.20	87.94	97.13	33.80	84.17	1.4134	4	Excellent
1.30	87.92	97.14	33.70	84.24	1.4150	4	Excellent
1.40	87.90	97.16	32.70	84.29	1.4288	4	Excellent
1.50	87.90	97.17	33.60	84.34	1.4168	4	Excellent
1.60	87.92	97.18	33.60	84.38	1.4171	4	Excellent
1.70	87.95	97.17	33.60	84.42	1.4174	4	Excellent
1.80	88.00	97.19	33.50	84.45	1.4191	4	Excellent
1.90	88.05	97.20	33.50	84.48	1.4195	4	Excellent
2.00	88.10	97.21	33.50	84.51	1.4198	4	Excellent

Table 15. The performance result with $k \in (2.0, 16.0)$.

k	PI plus FF Control						
	β_1 (%)	β_2 (%)	t_S (s)	K(%)	DPAI	Num	Performance
3.00	133.84	110.55	42.60	99.34	1.5859	4	Excellent
4.00	152.28	108.44	38.60	101.00	1.6866	4	Excellent
5.00	——※	——※	——※	——※	——※	0	Unacceptable
6.00	——※	——※	——※	——※	——※	0	Unacceptable
7.00	——※	——※	——※	——※	——※	0	Unacceptable
8.00	——※	——※	——※	——※	——※	0	Unacceptable
9.00	——※	——※	——※	——※	——※	0	Unacceptable
10.00	——※	——※	——※	——※	——※	0	Unacceptable
12.00	——※	——※	——※	——※	——※	0	Unacceptable
15.00	——※	——※	——※	——※	——※	0	Unacceptable
16.00	——※	——※	——※	——※	——※	0	Unacceptable

Note.※—— indicates that the system is unstable.

Table 16. The performance result with $k \in (2.0, 16.0)$.

k	IMC-PI Control						
	β_1 (%)	β_2 (%)	t_S (s)	K(%)	DPAI	Num	Performance
3.00	88.29	97.25	33.30	84.67	1.4240	4	Excellent
4.00	88.37	97.27	33.30	84.76	1.4248	4	Excellent
5.00	88.42	97.28	33.20	84.81	1.4266	4	Excellent
6.00	88.45	97.28	33.20	84.84	1.4268	4	Excellent
7.00	88.47	97.29	33.20	84.86	1.4270	4	Excellent
8.00	88.49	97.29	33.20	84.88	1.4272	4	Excellent
9.00	88.50	97.30	33.10	84.90	1.4287	4	Excellent
10.00	88.51	97.30	33.10	84.91	1.4288	4	Excellent
12.00	88.56	97.30	33.10	84.92	1.4290	4	Excellent
15.00	95.14	98.65	37.10	84.94	1.4058	4	Excellent
16.00	——※	——※	——※	——※	——※	0	Unacceptable

Note: ※—— indicates that the system is unstable.

(**a**) The power response with *k*=3.0 .

(**b**) The power response with *k*=4.0 .
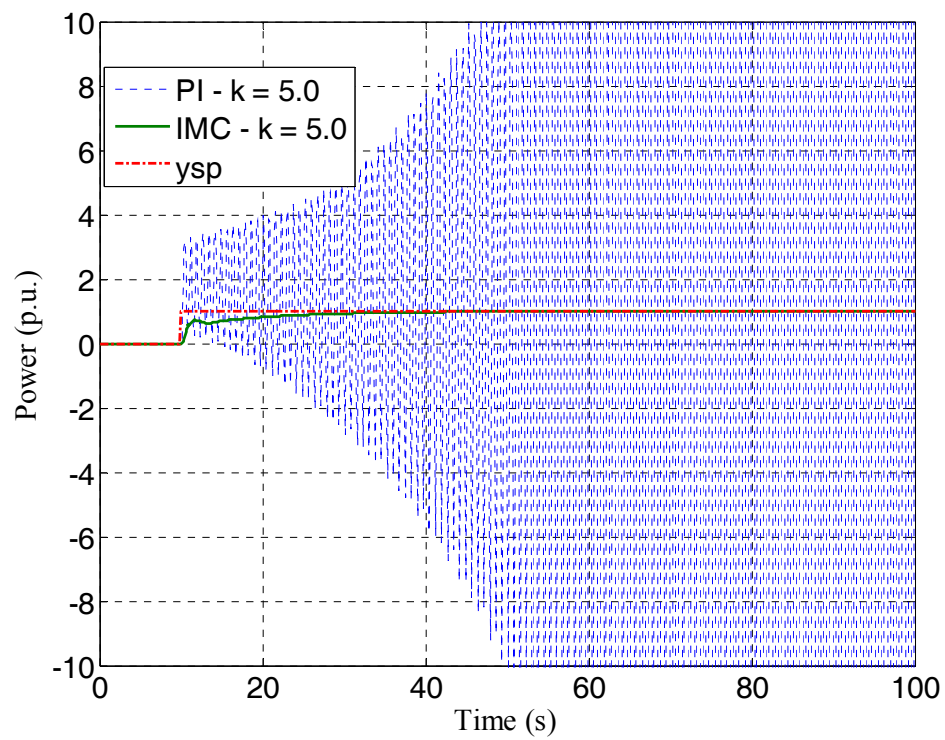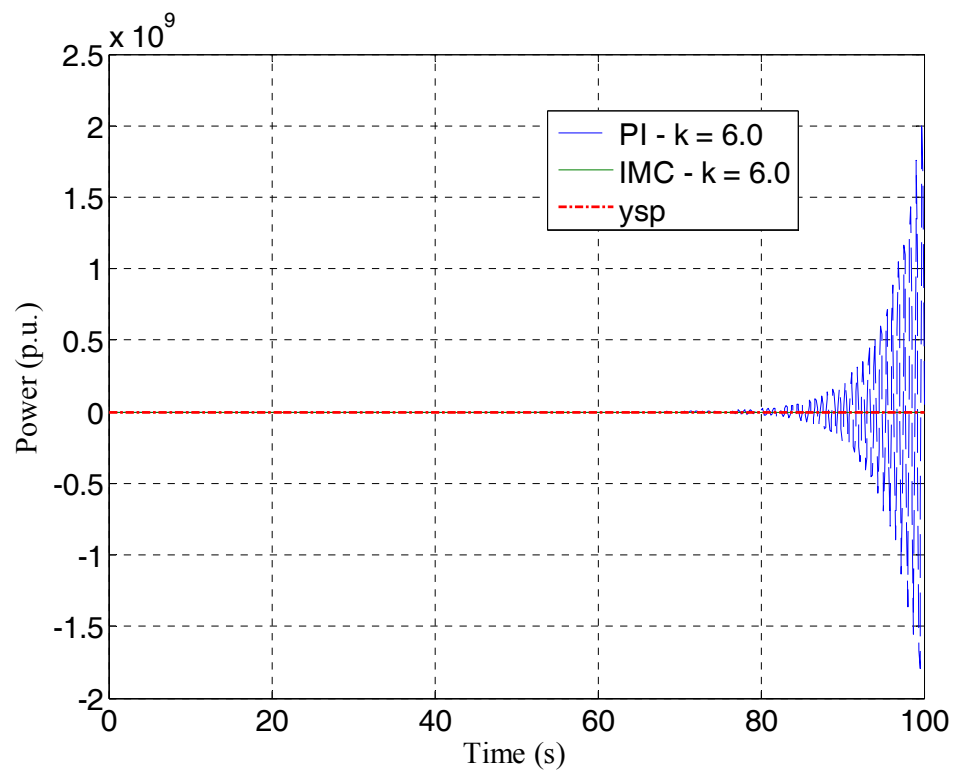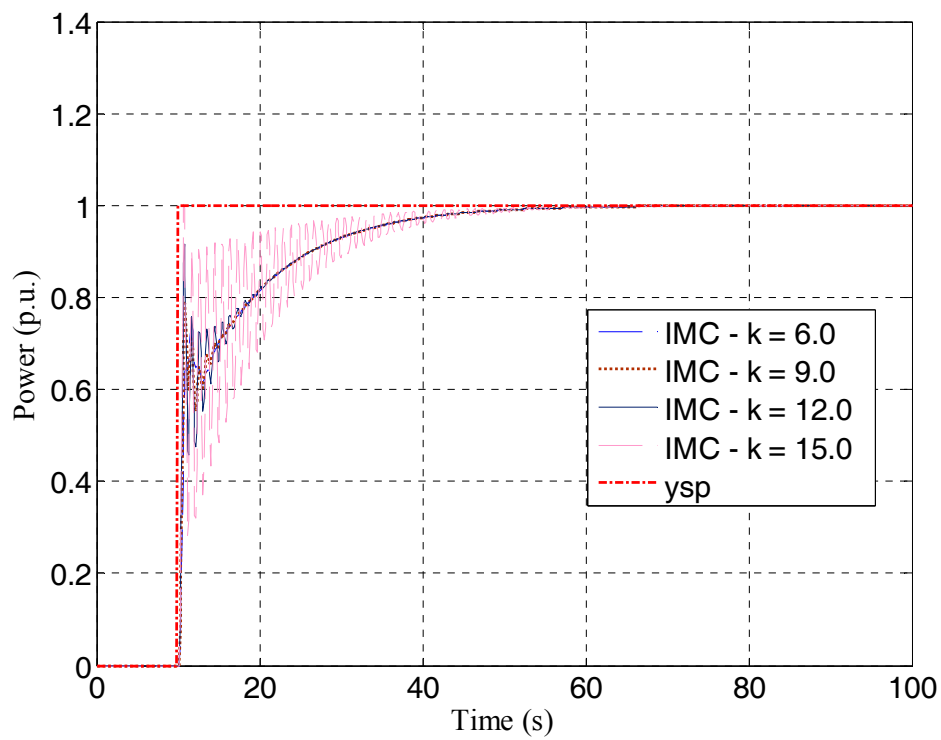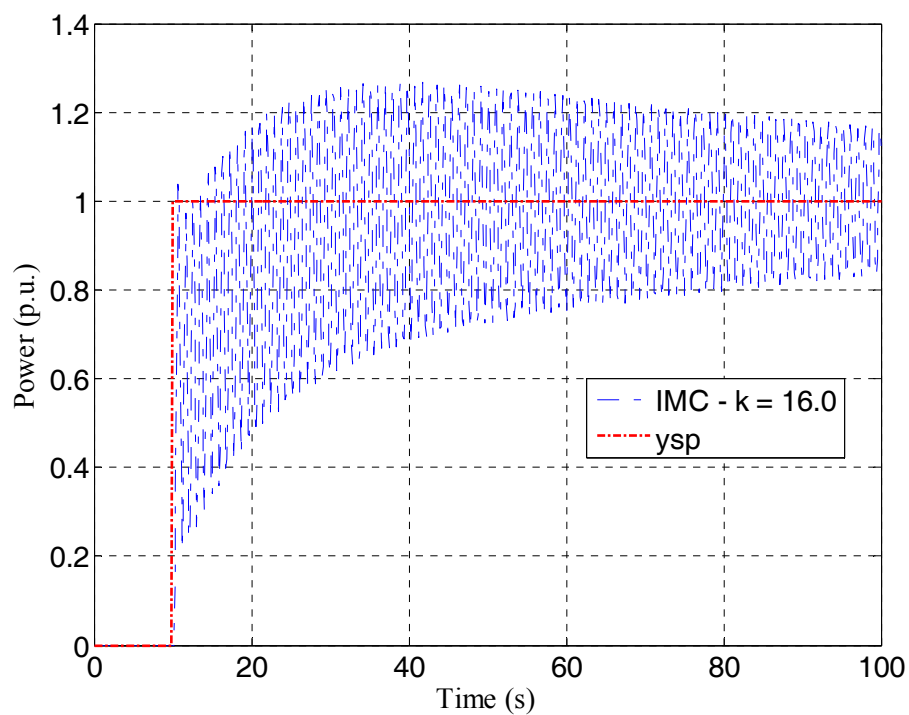
Figure 25. *Cont.*

(**c**) The power response with $k=5.0$.

(**d**) The power response with $k=6.0$.

Figure 25. *Cont.*

(**e**) The power response with $k \in (6.0, 15.0)$.

(**f**) The power response with $k = 16.0$.

Figure 25. The power response with $k \in (2.0, 16.0)$.

Figure 25, Table 15, and Table 16 show that, under $k \in (2.0, 16.0)$, the traditional PI plus FF power system control becomes unstable when $k \geq 5.0$, and the IMC one becomes unstable when $k \geq 16.0$,

so the system based on IMC can maintain stability and perform better in a larger parameter range. That is, the PCS based on IMC-PI is more robust than that based on PI-FF.

Through the simulation method, this section analyzes the robustness of PCS and the theoretical derivation and the assessment to this question will be carried out in the next section. When the local flow coefficient is the open-loop gain of the system, the root locus method is used to analyze the relationship between the stability of the system and this variable.

5.3. Closed Loop Characteristic Root Locus Assessment

The assessment of Section 5.2 shows that, when the k increases to a certain extent, the traditional PCS based on PI plus FF becomes unstable. Compared with the traditional system, the stability of PCS based on IMC-PI is analyzed. The controller parameters are the same as in Section 5.2.

The closed loop characteristic equation of traditional system based on PI plus FF is as follows:

$$Cha_{PI-FF}(s) = 1 + kG_T^*(s)G_{EN}(s) = 0. \tag{46}$$

Substitute the relevant parameters and Equations (30), (31), (34), (35), and (39) into Equation (46), the open-loop transfer function is obtained:

$$
\begin{aligned}
G_{Open-PI-FF}(s) &= G_T^*(s)G_{EN}(s) \\
&= \frac{12.98s^3 + 6.725s^2 + 1.07s + 0.05}{0.008182s^7 + 0.2903s^6 + 3.224s^5 + 20.15s^4 + 127.6s^3 + 22.48s^2 + s}
\end{aligned}
\tag{47}
$$

Compared with Equation (46), the closed loop characteristic equation of the PCS based on IMC-PI is as follows:

$$Cha_{IMC-PI}(s) == 1 + kG_{DT}(s)G_c(s)G_z(s)[1 - G_{IMC}(s) + G_T(s)G_{EN}(s)] = 0. \tag{48}$$

Similarly, the open loop transfer function corresponding to the IMC-PI control system is as follows:

$$
\begin{aligned}
G_{Open-IMC-PI}(s) &= G_{DT}(s)G_k(s)G_z(s)[1 - G_{IMC}(s) + G_T(s)G_{EN}(s)] \\
&= \frac{0.276s^7 + 6.636s^6 + 39.21s^5 + 707.8s^4 + 1486s^3 + 374.6s^2 + 33.3s + 1}{0.1702s^9 + 6.139s^8 + 70.67s^7 + 459.4s^6 + 2907s^5 + 2070s^4 + 427.2s^3 + 34.88s + s}
\end{aligned}
\tag{49}
$$

Let $k = 0 \rightarrow \infty$, the root locus of the traditional PI-FF and IMC-PI control system are, respectively, shown in Figures 26 and 27.

As can be seen from Figures 26 and 27 that the traditional PID control system is in critical oscillation when $k \approx 3.9734$, while the IMC system is in critical oscillation when $k \approx 15.3793$. This means that, when the local flow coefficient is too large, the new system is not prone to oscillate and the stability of the system is enhanced. The assessment of the closed-loop control system using the root locus method verifies the correctness of the simulation results in Section 5.2. Compared with the theoretical assessment, the simulation method is more intuitive and easy to understand for engineers.

The results of Sections 4 and 5 show that the performance assessment results based on IMC are obviously superior to traditional PI control. The main reason is that the control strategy based on IMC is more advanced in structure than traditional PI control, and its robustness is obviously stronger when the IM is established properly. When the characteristics of the controlled object change during operation, its adaptability is stronger too.
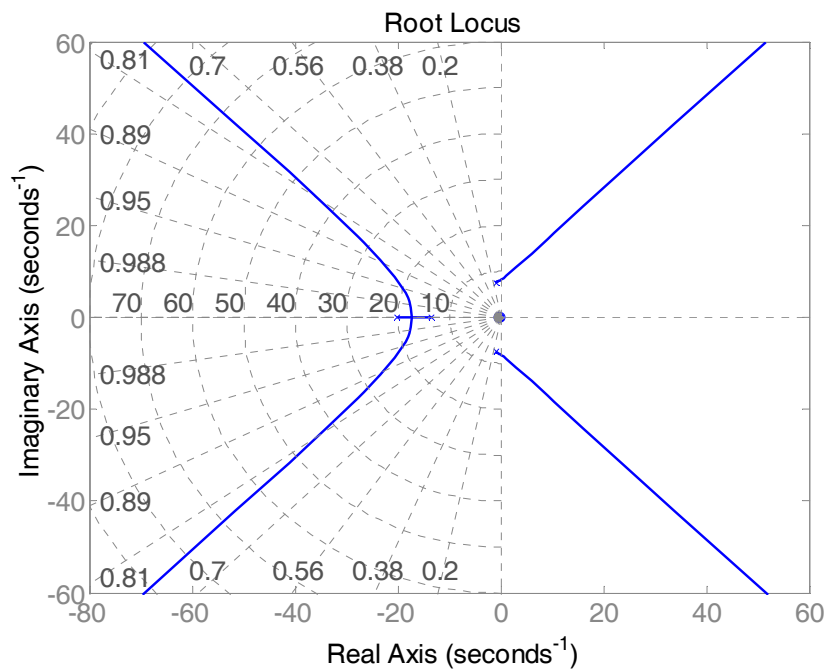
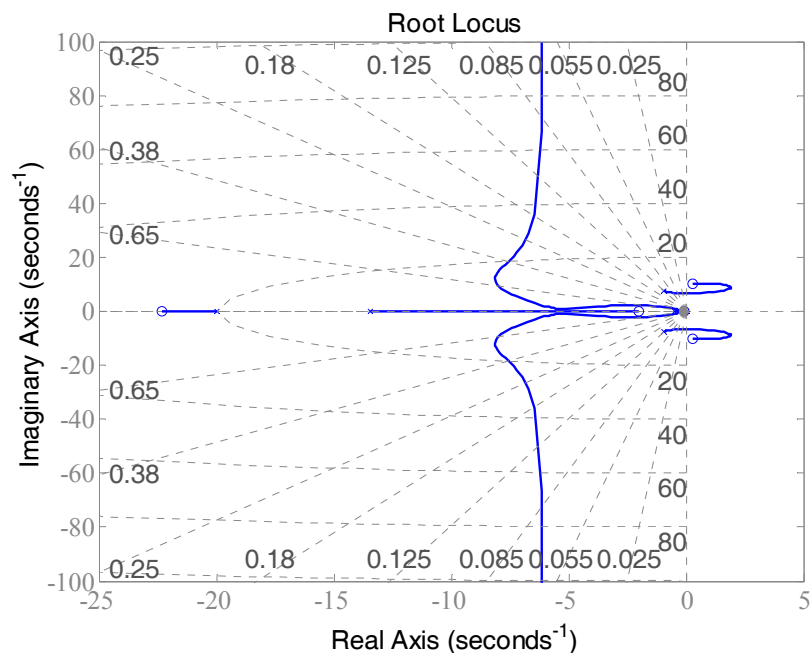**Figure 26.** Root locus of system based on PI-FF.

Figure 27. Root locus of system based on IMC-PI.

6. Conclusions

Firstly, according to the typical composition of the generating side of the power plant, the mathematical model of the PCS is established by the combination of theoretical assessment and system identification. At the same time, three typical control structures are given. Secondly, four dynamic performance indexes are given to evaluate the control performance of the PCS. A dynamic performance assessment index is defined by four dynamic performance indexes. At the same time, an auxiliary performance assessment index is given, and the benchmark and result of performance assessment are defined for the PCS. In a simulated environment, the performance of the PCS with different parameters was compared. According to the assessment results, the traditional PI controller combined with the FF

coefficient can achieve better performance. The combination of IMC and PI can also achieve better control performance, but the IMC is not suitable for adding FF coefficients. At the same time, the IMC combined with PI control mode achieved better overall performance than the traditional PI control mode. When tuning the parameters of the controller, despite the use of trial and error, which is slightly less theoretical, it can intuitively provide results to the engineers. Thirdly, the definition of the local flow coefficient of the valve is given. When the steam turbine is controlled in two different control modes, namely, the sequence valve and the single valve, the local flow coefficient is not completely consistent with the ideal linear characteristics. Therefore, in the same simulation environment, the influence of valve local flow coefficient on the robustness of PCS is analyzed. At the same time, when the PCS is in a critical stable state, the root locus assessment method is used. The numerical results also show that the IMC combined with PI is more robust than the traditional PI plus FF control strategy.

It should be noted that the application of IMC in power plant is not as wide as that of traditional PI. The reason is that the parameter tuning of IMC is more complex, while the parameter tuning of traditional PI controller is more mature. All these limit the wide application of IMC in power plants with emphasis on safety. In this paper, combined with a trial-and-error method and an optimization algorithm, the parameters of the PI controller are adjusted, which provides technical support for the wide application of IMC in practical power plants. Future research mainly includes three aspects: firstly, to establish a more accurate model of PCS; secondly, to study how to establish a better performance control strategy through simulation technology; finally, to find new problems of various new control strategies through field application in power plants.

Author Contributions: S.L. and Y.W. conceived and designed the experiments; S.L. performed the experiments; S.L. and Y.W. analyzed the data; Y.W. contributed analysis tools; S.L. wrote the paper.

Conflicts of Interest: The authors declare no conflicts of interest.

Abbreviations

AGC	Automatic Generation Control
DPAI	Dynamic Performance Assessment Index
FF	Feed Forward
FFC	Feed Forward Control
IM	Internal Model
IMC	Internal Model Control
PF	Primary Frequency
PFM	Primary Frequency Modulation
P	Proportion
PI	Proportion Integration
PD	Proportion Differentiation
PID	Proportion Integration Differentiation
PCS	Power Control System
LSE	Least Square Estimation
LSM	Least Square Method

Appendix A

Table A1. Parameters of the steam turbine governing system model.

Description	Identification	Parameter Value
Proportional coefficient of electro-hydraulic servo system	K_{P1}	12.0
Integral coefficient of electro-hydraulic servo system	K_{I1}	1.00
Time constant of oil motive	T	0.889
Power coefficient of high pressure cylinder	F_{HP}	0.281
Power coefficient of medium pressure cylinder	F_{IP}	0.30
Power coefficient of low pressure cylinder	F_{LP}	0.419
Time constant of high pressure chamber volume	T_{CH}	0.0498
Time constant of reheated steam chamber volume	T_{RH}	10.40
Time constant of connected pipe volume	T_{CO}	0.10
Power overshoot coefficient of high pressure cylinder	λ	0.85

Appendix B

Mathematical Model of Synchronous Generator in Thermal Power Unit: A Sixth-Order Differential Equation.

$$T'_{d0} \frac{dE'_q}{dt} = E_{fd} - (x_d - x'_d)I_d - E'_q \tag{A1}$$

$$T''_{d0} \frac{dE''_q}{dt} = -E''_q - (x'_d - x''_d)I_d + E'_q + T''_{d0} \frac{dE'_q}{dt} \tag{A2}$$

$$T'_{q0} \frac{dE'_d}{dt} = -E'_d + (x_q - x'_q)I_q \tag{A3}$$

$$T''_{q0} \frac{dE''_d}{dt} = -E''_d + (x'_q - x''_q)I_q + E'_d + T''_{q0} \frac{dE'_d}{dt} \tag{A4}$$

$$T_J \frac{d\omega}{dt} = M_m - M_e - D(\omega - \omega_0) \tag{A5}$$

$$\frac{d\delta}{dt} = \omega - \omega_0. \tag{A6}$$

Equations (A1)–(A4) are output power and the electromagnetic torque equations presented, respectively, on *d* and *q* axes. Equations (A5) and (A6) are the scalar form of the rotor motion equation for synchronous motors. Equation (A6) is the rotor angular motion equation.

References

1. Zhang, Y.; Gao, K.; Qu, Z. An evaluation method of primary frequency modulation performance based on characteristics of unit output power curves. *Dianli Xitong Zidonghua/Autom. Electr. Power Syst.* **2012**, *36*, 99–103.
2. Delavari, A.; Kamwa, I. Improved optimal decentralized load modulation for power system primary frequency regulation. *IEEE Trans. Power Syst.* **2018**, *33*, 1013–1025. [CrossRef]
3. Tavakkoli, M.; Adabi, J.; Zabihi, S.; Godina, R.; Pouresmaeil, E. Reserve Allocation of Photovoltaic Systems to Improve Frequency Stability in Hybrid Power Systems. *Energies* **2018**, *11*, 2583. [CrossRef]
4. Tavakoli, M.; Pouresmaeil, E.; Adabi, J.; Godina, R.; Catalão, J.P. Load-frequency control in a multi-source power system connected to wind farms through multi terminal HVDC systems. *Comput. Oper. Res.* **2018**, *96*, 305–315. [CrossRef]
5. Choi, Y.G.; Lee, S.; Lee, H.S.; Lee, S.C.; Kang, B. Increase in power conversion efficiency of bidirectional DC-DC converter using 1:1 transformer and pulse frequency modulation control. *IEEE Trans. Power Electron.* **2018**, *33*, 10539–10549. [CrossRef]
6. Choi, H.J.; Jung, J.H. Enhanced power line communication strategy for DC microgrids using switching frequency modulation of power converters. *IEEE Trans. Power Electron.* **2017**, *32*, 4140–4144. [CrossRef]
7. Ahmed, A.M.H.E. Boiler Control Design Using Fuzzy Logic. Ph.D. Thesis, Sudan University of Science and Technology, Khartoum, Sudan, 2017.

8.　Ławryńczuk, M. Nonlinear predictive control of a boiler-turbine unit: A state-space approach with successive on-line model linearisation and quadratic optimisation. *ISA Trans.* **2017**, *67*, 476–495. [CrossRef]

9.　Paul, A.; Joos, G.; Kamwa, I. Dynamic state estimation of full power plant model from terminal phasor measurements. In Proceedings of the 2018 IEEE/PES Transmission and Distribution Conference and Exposition (T&D), Denver, CO, USA, 16–19 April 2018; pp. 1–5.

10.　Gomez-Exposito, A.; Conejo, A.J.; Canizares, C. *Electric Energy Systems: Analysis and Operation*; CRC Press: Boca Raton, FL, USA, 2018.

11.　Wang, P.; Liu, Y. Influence of a circular strainer on unsteady flow behavior in steam turbine control valves. *Appl. Therm. Eng.* **2017**, *115*, 463–476. [CrossRef]

12.　Wang, J.; Ma, Q.; Zhong, J.; Gou, X. Mechanism research on active power fluctuation caused by steam turbine valve test. *Electr. Eng.* **2018**, *100*, 2147–2154. [CrossRef]

13.　Nan, D.; Guosheng, L.; Yushan, W. Research on Primary Frequency Modulation Function Operating on Large Fossil-fuel Power Plants. *North China Electr. Power* **2003**, *10*, 000.

14.　Molina-Garcia, A.; Bouffard, F.; Kirschen, D.S. Decentralized demand-side contribution to primary frequency control. *IEEE Trans. Power Syst.* **2011**, *26*, 411–419. [CrossRef]

15.　Shang, X.; Li, L.; Zhuo, J.; Yang, X.; Luo, Y.; Liu, G. Improvement of Strategies of AGC in North China Power Grid After UHVAC Pilot Project Operation. *Power Syst. Technol.* **2010**, *9*, 007.

16.　Shabani, H.; Vahidi, B.; Ebrahimpour, M. A robust PID controller based on imperialist competitive algorithm for load-frequency control of power systems. *ISA Trans.* **2013**, *52*, 88–95. [CrossRef] [PubMed]

17.　Liu, K.; Wang, S.; Wu, Q.; Wang, L.; Ma, Q.; Zhang, L.; Li, G.; Tian, H.; Duan, L.; Hao, J. A Highly Resolved Mercury Emission Inventory of Chinese Coal-Fired Power Plants. *Environ. Sci. Technol.* **2018**, 2400–2408. [CrossRef] [PubMed]

18.　Yang, J. Research and development of assessment system of primary frequency regulation in central China power grid. *Autom. Electr. Power Syst.* **2008**, *9*, 024.

19.　Gu, Y.; Xu, J.; Chen, D.; Wang, Z.; Li, Q. Overall review of peak shaving for coal-fired power units in China. *Renew. Sustain. Energy Rev.* **2016**, *54*, 723–731. [CrossRef]

20.　Jin, N.; Liu, W.Y.; Cao, Y.L.; Xing, Z.; Cui, G. Influence on the grid frequency characteristic by the parameters of primary frequency modulation of large capacity generator units. *Power Syst. Prot. Control* **2012**, *40*, 91–95.

21.　Zimmer, G. Modelling and simulation of steam turbine processes: Individual models for individual tasks. *Math. Comput. Model. Dyn. Syst.* **2008**, *14*, 469–493. [CrossRef]

22.　Sheng, K.; Liu, F.; Liu, W.; Xun, X.; Wang, B.; Li, J. Influence of steam turbine valve discharge characteristics on power systems and its control strategy. *Dianli Xitong Zidonghua/Autom. Electr. Power Syst.* **2012**, *36*, 104–109.

23.　Wen, X.K.; Zhong, J.L.; Qian, J. Research on the control strategy for turbine on low-frequency oscillation. *Proc. CSEE* **2009**, *26*, 020.

24.　Ke, Y. Design of IMC Oriented PID Control Law for Typical Thermal Process in Thermal Power Plant. *Energy Fuel Technol.* **2018**. [CrossRef]

25.　Dos Santos, L.R.; Durand, F.R.; Goedtel, A.; Abrão, T. Auto-tuning PID distributed power control for next-generation passive optical networks. *IEEE/OSA J. Opt. Commun. Netw.* **2018**, *10*, D110–D125. [CrossRef]

26.　Wu, X.; Shen, J.; Li, Y.; Wang, M.; Lawal, A. Flexible operation of post-combustion solvent-based carbon capture for coal-fired power plants using multi-model predictive control: A simulation study. *Fuel* **2018**, *220*, 931–941. [CrossRef]

27.　Kaushaley, S.; Shaw, B. Transient Analysis of Quasi Oppositional Based Lightning Search Algorithm Optimized PID Controller in Isolated Small Hydro Power Plant. *Trends Renew. Energy* **2018**, *4*, 34–43. [CrossRef]

28.　Garcia, C.E.; Morari, M. Internal model control. A unifying review and some new results. *Ind. Eng. Chem. Process Des. Dev.* **1982**, *21*, 308–323. [CrossRef]

29.　Saxena, S.; Hote, Y.V. Internal model control based PID tuning using first-order filter. *Int. J. Control Autom. Syst.* **2017**, *15*, 149–159. [CrossRef]

30.　Sonker, B.; Kumar, D.; Samuel, P. Design of two degree of freedom-internal model control configuration for load frequency control using model approximation. *Int. J. Model. Simul.* **2018**, 1–11. [CrossRef]

31.　Zahedi, F.; Zahedi, Z. A review of neuro-fuzzy systems based on intelligent control. *J. Electr. Electron. Eng.* **2015**, *3*, 58–61. [CrossRef]

32. Mars, P. *Learning Algorithms: Theory and Applications in Signal Processing, Control and Communications*; CRC Press: Boca Raton, FL, USA, 2018.

33. Mi, Y.; Zhang, H.; Fu, Y.; Wang, C.; Loh, P.C.; Wang, P. Intelligent Power Sharing of DC Isolated Microgrid Based on Fuzzy Sliding Mode Droop Control. *IEEE Trans. Smart Grid* **2018**. [CrossRef]

34. Babahajiani, P.; Shafiee, Q.; Bevrani, H. Intelligent demand response contribution in frequency control of multi-area power systems. *IEEE Trans. Smart Grid* **2018**, *9*, 1282–1291. [CrossRef]

35. Liu, Y.; Yan, Y.; Xu, M.; Song, K.; Shi, Q. Exact generator and its high order expansions in the time-convolutionless generalized master equation: Applications to the spin-boson model and exictation energy transfer. *Chin. J. Chem. Phys.* **2018**, *31*. [CrossRef]

36. Kanimba, E.; Pearson, M.; Sharp, J.; Stokes, D.; Priya, S.; Tian, Z. A comprehensive model of a lead telluride thermoelectric generator. *Energy* **2018**, *142*, 813–821. [CrossRef]

37. Wang, H.; Su, X.L. Several improvements of Prony algorithm and its application in monitoring low-frequency oscillations in power system. *Power Syst. Prot. Control* **2011**, *39*, 140–145.

38. Anna, L.; Xi, W.; Ping, J. Research on identifying low frequency oscillation modes based on morphological filtering theory and Prony algorithm. *Power Syst. Prot. Control* **2015**, *43*, 137–142.

39. Gu, Y.; Bottrell, N.; Green, T.C. Reduced-order models for representing converters in power system studies. *IEEE Trans. Power Electron.* **2018**, *33*, 3644–3654. [CrossRef]

40. Zhou, K.; Yang, S. Demand side management in China: The context of China's power industry reform. *Renew. Sustain. Energy Rev.* **2015**, *47*, 954–965. [CrossRef]

41. Yuan, J.; Shen, J.; Pan, L.; Zhao, C.; Kang, J. Smart grids in China. *Renew. Sustain. Energy Rev.* **2014**, *37*, 896–906. [CrossRef]

42. Xie, X.; Xin, Y.; Xiao, J.; Wu, J.; Han, Y. WAMS applications in Chinese power systems. *IEEE Power Energy Mag.* **2006**, *4*, 54–63.

43. Aström, K.J.; Hägglund, T. *PID Controllers: Theory, Design, and Tuning*; Instrument Society of America: Research Triangle Park, NC, USA, 1995; p. 67.

44. Kaya, I. Simple and optimal PI/PID tuning formulae for unstable time delay processes. In Proceedings of the 2017 10th International Conference on Electrical and Electronics Engineering (ELECO), Bursa, Turkey, 30 November–2 December 2014; pp. 847–851.

45. Ozyetkin, M.M.; Onat, C.; Tan, N. PID Tuning Method for Integrating Processes Having Time Delay and Inverse Response. *IFAC-PapersOnLine* **2018**, *51*, 274–279. [CrossRef]